https://doi.org/10.5194/se-2020-104
Preprint. Discussion started: 14 July 2020


Solid Earth Discussions

# A systems-based approach to parameterise seismic hazard in regions with little historical or instrumental seismicity: The South Malawi Active Fault Database

Jack N. Williams[a*], Hassan Mdala[b], Åke Fagereng[a], Luke N.J. Wedmore[c], Juliet Biggs[c], Zuze Dulanya[d], Patrick Chindandali[e], Felix Mphepo[b]

**Affiliations**

[a]*School of Earth and Ocean Sciences, Cardiff University, Cardiff, UK*

[b]*Geological Survey Department, Mzuzu Regional Office, Mzuzu, Malawi*

[c]*School of Earth Sciences, University of Bristol, Bristol, UK*

[d]*Geography and Earth Sciences Department, University of Malawi, Zomba, Malawi*

[e]*Geological Survey Department, Zomba, Malawi*

*Corresponding author: Jack Williams (williamsj132@cardiff.ac.uk)

**Abstract**

Seismic hazard is frequently characterised using instrumental seismic records. However, in regions where the instrumental record is short relative to earthquake repeat times, extrapolating it to estimate seismic hazard can misrepresent the probable location, magnitude, and frequency of future large earthquakes. Although paleoseismology can address this challenge, this approach requires certain geomorphic settings and carries large inherent uncertainties. Here, we outline how fault slip rates and recurrence intervals can be estimated through an approach that combines fault geometry, earthquake-scaling relationships, geodetically derived regional strain rates, and geological constraints of regional strain distribution. We then apply this approach to the southern Malawi Rift where, although no on-fault slip rate measurements exist, there are theoretical and observational

https://doi.org/10.5194/se-2020-104
Preprint. Discussion started: 14 July 2020


constraints on how strain is distributed between border and intrabasinal faults. This has led to the development of the South Malawi Active Fault Database (SMAFD), the first database of its kind in the East African Rift System (EARS) and designed so that the outputs can be easily incorporated into Probabilistic Seismic Hazard Analysis. We estimate earthquake magnitudes of $M_W$ 5.4-7.2 for individual fault sections in the SMAFD, and $M_W$ 6.0-7.8 for whole fault ruptures. These potentially high magnitudes for continental normal faults reflect southern Malawi's 11-140 km long faults and thick (30-35 km) seismogenic crust. However, low slip rates (intermediate estimates 0.05-0.8 mm/yr) imply long recurrence intervals between events: $10^2$-$10^5$ years for border faults and $10^3$-$10^6$ years for intrabasinal faults. Sensitivity analysis indicates that the large range of these estimates can be reduced most significantly from an improved understanding of the rate and partitioning of rift-extension in southern Malawi, earthquake scaling relationships, and earthquake rupture scenarios. Hence these are critical areas for future research. The SMAFD provides a framework for using geological and geodetic information to characterize seismic hazard in low strain rate settings with few on-fault slip rate measurements, and could be adapted for use elsewhere in the EARS or globally.

## 1. Introduction

Earthquake ruptures tend to occur on pre-existing faults (Brace and Byerlee, 1966; Jackson, 2001; Scholz, 2002; Sibson, 1989). Thus, the identification and systematic mapping of active faults, which are then compiled with other fault attributes (e.g. slip rate and slip sense) into a geospatial active fault database, provides an important tool in assessing regional seismic hazard (Christophersen et al., 2015; Hart and Bryant, 1997; Langridge et al., 2016; Shyu et al., 2016; Styron et al., 2020; Taylor and Yin, 2009). Not only can these databases inform on the surface rupture risk (Hart and Bryant, 1997; Villamor et al., 2012), they can also be converted into earthquake sources for Probabilistic Seismic Hazard Assessment (PSHA) to forecast future levels of ground shaking (e.g. Beauval et al.,

https://doi.org/10.5194/se-2020-104
Preprint. Discussion started: 14 July 2020


2018; Hodge et al., 2015; Stirling et al., 2012). Furthermore, the data contained in active fault databases are inherently useful in understanding regional geological evolution (Agostini et al., 2011b; Basili et al., 2008; Taylor and Yin, 2009).

Despite their benefits, active fault databases have yet to be developed for many seismically active regions (Christophersen et al., 2015). This partly reflects the difficulty in estimating fault slip rates and earthquake recurrence intervals, as instrumental seismic records typically cover only a fraction of a fault's seismic cycle (Stein et al., 2012), whilst obtaining these attributes from dating offset surfaces and/or paleoseismology requires certain geomorphic settings and can involve large uncertainties (Cowie et al., 2012; McCalpin, 2009; Nicol et al., 2016b). Alternatively, decadal time-scale fault slip rates can be estimated using geodetic estimates and block models where the crust is divided by mapped faults (e.g. Field et al., 2014; Wallace et al., 2012; Zeng and Shen, 2014). However, not all plate boundaries are covered by sufficiently dense geodetic networks to perform this analysis, and/or sometimes geodetic data cannot resolve how strain is distributed (Calais et al., 2016; Stein et al., 2012).

In this study, by combining geodetic and geological information, we present a new systems-based approach to estimate slip rates and earthquake recurrence intervals within narrow (<100 km width; Buck, 1991) amagmatic continental rifts. However, this method could be adapted for any region with low strain rates, well developed active fault maps, and an understanding of strain partitioning. We then apply this method to southern Malawi, which has culminated in the development of the South Malawi Active Fault Database (SMAFD).

The SMAFD represents the first active fault database to be developed within the East African Rift System (EARS), where population growth and seismically vulnerable building stock is driving an

https://doi.org/10.5194/se-2020-104
Preprint. Discussion started: 14 July 2020



increased exposure to seismic hazard (World Bank, 2019; Goda et al., 2016; Hodge et al., 2015; Kloukinas et al., 2019; Ngoma et al., 2019; Novelli et al., 2019). Notably, previous PSHA in the EARS has typically been conducted using the ~65 year long instrumental record of seismicity alone (Ayele, 2017; Goitom et al., 2017; Midzi et al., 1999; Poggi et al., 2017). However, low EARS strain rates (regional extension rates ~1-6 mm/yr; Stamps et al., 2018) imply that this record is incomplete and may underestimate seismicity rates compared to those inferred from geodesy and paleoseismology (Ebinger et al., 2019; Hodge et al., 2015; Stein et al., 2012; Vallage and Bollinger, 2019). Hence, by providing more complete earthquake sources for PSHA, active fault databases in the EARS may play an important role in characterising its ever-increasing seismic risk (Goda et al., 2016; Hodge et al., 2015).

Southern Malawi lies at the southern incipient end of the EARS where the rift floor is nearly entirely onshore, follows regional Proterozoic fabrics, and is not buried by magmatism or significant amounts of sediments (Wedmore et al., 2020a, 2020b; Williams et al., 2019). The SMAFD therefore also provides constraints on faulting during the early stages of continental rifting and the influence of pre-existing mechanical anisotropies in the crust on fault evolution.

This study first describes the seismotectonic setting of southern Malawi (Sect. 2), and the approach used for mapping its active faults (Sect. 3). In Sect. 4 we then describe the method used to estimate fault slip rates, earthquake magnitudes and recurrence intervals, using southern Malawi as an example. Results from the SMAFD are documented in Sect. 5 along with an evaluation of fault slip rate estimates and a sensitivity analysis. Finally, in Sect. 6, we discuss the implication of the SMAFD in terms of fault growth in continental rifts, southern Malawi's seismic hazard, and the strategies needed to reduce uncertainties when assessing this hazard.

https://doi.org/10.5194/se-2020-104
Preprint. Discussion started: 14 July 2020



## 2. Southern Malawi seismotectonics

### *2.1 Tectonic history of southern Malawi*

Southern Malawi lies at a complex intersection of orogenic belts that formed during the Pan African Orogeny (~800-450 Ma) and possibly earlier Irumide age deformation (~1,020-950 Ma) as the African continent gradually amalgamated during the Proterozoic, and which imparted amphibolite-granulite facies metamorphic fabrics (mineral segregations and alignments) within the rift's basement rocks (Figs. 1 and 2; Andreoli, 1984; Fritz et al., 2013; Fullgraf et al., 2017; Kröner et al., 2001; Manda et al., 2019). Within the Phanerozoic (540 Ma to present day), Permian-Triassic sediments were deposited in the Lower Shire Graben under NW-SE Karoo extension (Fig. 1b; Castaing, 1991; Habgood et al., 1973; Wedmore et al., 2020b). NE-SW striking dykes then formed during the Jurassic, followed by minor accumulations of Cretaceous sediments under NE-SW extension (Castaing, 1991). Evidence for Upper Jurassic to Cretaceous magmatism is also observed across southern Malawi with the emplacement of the Chilwa Alkaline Province (Bloomfield, 1965; Dulanya, 2017; Eby et al., 1995; Manda et al., 2019).

### *2.2 Southern Malawi tectonic setting*

Southern Malawi lies towards the southern incipient end of the EARS Western Branch, where it represents the divergent boundary between the Rovuma and Nubia plates (Fig. 1; Saria et al., 2013; Stamps et al., 2008, 2018). The rift itself consists principally of three linked 50-150 km long grabens and half grabens that follow regional Proterozoic fabrics and channel the Shire River, Lake Malawi's only outlet, towards its confluence with the Zambezi River (Figs. 1 and 2; Chapola and Kaphwiyo, 1992; Dulanya, 2017; Ebinger, 1989; Ebinger et al., 1987; Ivory et al., 2016; Wedmore et al., 2020a; Williams et al., 2019). Like elsewhere in the Western Branch, each of these grabens is defined by one or more border faults, whose footwall escarpments dominate the topographic expression of the rift (Ebinger, 1989).

https://doi.org/10.5194/se-2020-104
Preprint. Discussion started: 14 July 2020



Border fault footwall escarpments in southern Malawi tend to be 300-1000 m high (Figs. 2 and 3; Laõ-Dávila et al., 2015; Wedmore et al., 2020a, 2020b), and so are lower than in northern Malawi (1000-2000 m; Accardo et al., 2018; Flannery and Rosendahl, 1990; Laõ-Dávila et al., 2015). Furthermore, in central and northern Malawi, the rift is occupied by Lake Malawi and a <5 km thick synrift sedimentary sequence (Accardo et al., 2018). Conversely, the floors of the grabens in southern Malawi are subaerially exposed except for the 450 $km^2$ flooded by Lake Malombe. Boreholes and electrical resistivity surveys suggest that alluvial and colluvial sediments that cover the basement in the Zomba and Makanjira grabens are <100 m thick (Fig. 2b; Bloomfield and Garson, 1965; King and Dawson, 1976; Mynatt et al., 2017; Walshaw, 1965; Walter, 1972). Cumulatively, these observations indicate that the rift in southern Malawi has accommodated less extensional strain than further north. Therefore, although the age of EARS rifting in southern Malawi is poorly constrained (Dulanya, 2017; Wedmore et al., 2020a), it is unlikely to be older than the mid-Pliocene (~4.5 Ma) onset of sediment accumulation in Lake Malawi (Delvaux, 1995; McCartney and Scholz, 2016), and almost certainly not older than the Oligocene (23-25 Ma) age of the northern end of the Malawi Rift (Mesko, 2020; Mortimer et al., 2016; Roberts et al., 2012). However, it is unclear if the rift in southern Malawi is actually younger than in northern Malawi, and/or it is the same age but has been extending at a slower rate due to its proximity to the Nubia-Rovuma Euler pole (Fig. 1a).

The floors of the Zomba and Makanjira graben sit at an altitude only ~10 m higher than Lake Malawi. Hence, the sediments deposited in these grabens likely formed during base level changes in lake level, when it was up to 150 m higher than present (Ivory et al., 2016; Lyons et al., 2015; McCartney and Scholz, 2016), and would have flooded this section of the rift (Wedmore et al., 2020a). Between the Zomba and Lower Shire grabens, the rift floor elevation drops from ~450 to

~100 m; however, there is no evidence that this is controlled by active faults (Dulanya, 2017; Wedmore et al., 2020a). The Rungwe Volcanic Province, the closest EARS volcanism to southern Malawi, is ~700 km to the north (Fig. 1a), and hot springs in southern Malawi do not indicate a magmatic origin (Dulanya et al., 2010). Nevertheless, minor intrusions into the lower crust cannot be excluded (Wang et al., 2019).

Prior to this study, the only systematic active fault mapping in southern Malawi was conducted by Castaing (1991) and Chapola and Kaphwiyo (1992), whose maps were subsequently incorporated by Macgregor (2015) into EARS scale maps, and later into the Global Earthquake Model (GEM) Global Active Faults map (Fig. 2b; https://blogs.openquake.org/hazard/global-active-fault-viewer/, date last accessed 4 June 2020). However, the faults are mapped at a coarse scale, and there is no additional information such as slip rates or evidence for recent fault activity that are both vital components of an active fault database.

### *2.3 Southern Malawi seismicity*

There are no known historical accounts of surface rupturing earthquakes in southern Malawi, although a continuous written record only extends to c. 1870 (Pike, 1965; Stahl, 2010). However, in northern Malawi, the previously unrecognised St Mary fault exhibited surface rupture following the 2009 Karonga earthquake sequence (Fig. 1b; Hamiel et al., 2012; Kolawole et al., 2018b; Macheyeki et al., 2015). This sequence primarily consisted of four shallow (focal depths <8 km) $M_W$ 5.5-5.9 events over a 13 day period (Biggs et al., 2010; Gaherty et al., 2019). Another relevant event for southern Malawi is the 1910 $M_S$ 7.4 Rukwa Earthquake in southern Tanzania (Ambraseys, 1991). The fault source for this event is not certain, though the Kanda fault is a likely candidate (Vittori et al., 1997), and its steep and laterally continuous scarp closely resembles that of some faults in southern Malawi (Hodge et al., 2018a, 2019, 2020; Wedmore et al., 2020a, 2020b).

https://doi.org/10.5194/se-2020-104
Preprint. Discussion started: 14 July 2020



The largest instrumentally recorded earthquake in southern Malawi is a M 6.7 event in 1954 (De Bremaeker, 1956; Delvaux and Barth, 2010). The International Seismological Centre (ISC) record for Malawi is complete for events with magnitude ($M_W$) > 4.5 to 1965 (Figs. 1b and 2a; Hodge et al., 2015), with the largest event in this record being the 1989 $M_W$ 6.3 Salima Earthquake (Jackson and Blenkinsop, 1993). Notably, seismicity in Malawi is commonly observed to depths far greater (30-35 km; Craig et al., 2011; Delvaux and Barth, 2010; Jackson and Blenkinsop, 1993) than would be expected for continental crust of typical composition and geothermal gradient (10-15 km). Thick cold anhydrous lower crust (Craig et al., 2011; Jackson and Blenkinsop, 1997; Nyblade and Langston, 1995), localised weak viscous zones embedded within strong lower crust (Fagereng, 2013), and/or volumes of mafic material in the lower crust (Shudofsky et al., 1987) that are velocity weakening at temperatures <700 °C (Hellebrekers et al., 2019) have been proposed as explanations for this unusually deep seismicity.

### *2.4 Estimates of stress and strain in southern Malawi*

Earthquake focal mechanism stress inversions for the entire Malawi Rift indicate a normal fault stress state (i.e. vertical maximum principal compressive stress) with an ENE-WSW to E-W trending minimum principal compressive stress ($\sigma_3$; Fig. 1b Delvaux and Barth, 2010; Ebinger et al., 2019; Williams et al., 2019). This $\sigma_3$ orientation is comparable to the $\sigma_3$ direction inferred from regional joint orientations (Williams et al., 2019), and the geodetically-derived extension direction between the Nubia and Rovuma plates (Fig. 1b; Saria et al., 2014; Stamps et al., 2018). ENE-WSW to E-W extension indicates that NE-SW striking faults in Malawi should accommodate oblique slip. However, slickensides and earthquake focal mechanisms indicate approximately dip-slip motion regardless of fault strike in southern Malawi (Fig. 1b; Delvaux and Barth, 2010; Hodge et al., 2015; Wedmore et al., 2020a). This apparent inconsistency between faults that are simultaneously

https://doi.org/10.5194/se-2020-104
Preprint. Discussion started: 14 July 2020

Solid Earth Discussions

accommodating near pure dip-slip and strike oblique to the regional extension direction can be explained if the lower crust in southern Malawi contains lateral rheological heterogeneities such as an anastomosing shear zone (Fagereng, 2013; Hodge et al., 2018a; Philippon et al., 2015; Wedmore et al., 2020a; Williams et al., 2019).

*2.5 Seismic hazard assessment in southern Malawi*

Using instrumental catalogues, PSHA have been conducted for southern Malawi as part of EARS-wide studies (Midzi et al., 1999; Poggi et al., 2017). These indicate that there is a 10% probability of exceeding 0.15 g peak ground acceleration in southern Malawi in the next 50 years (Poggi et al., 2017). However, the rift extension rate calculated from the seismic moment release rate in Malawi (0.3 mm/yr; Hodge et al., 2015) is less than the geodetically estimated extension rate (~0.5-2 mm/yr; Saria et al., 2013, 2014; Stamps et al., 2018). This implies that stress is accumulating in the crust that has not been released in earthquake ruptures during the relatively short instrumental time (Ebinger et al., 2019; Hodge et al., 2015). Thus, the geodetic and geomorphological information incorporated into SMAFD may be a better guide to the magnitude and locations of future seismicity in southern Malawi.

## 3. Mapping active faults in the SMAFD

An active fault database consists of an active fault map, where for each fault, attributes are added that detail geomorphic and geological information about the fault, and estimates of the parameters required to incorporate them as earthquake sources in PSHA (Christophersen et al., 2015). Typically, an active fault database is stored in a Geographic Information System (GIS) environment, in which the fault attributes are assigned to a linear feature that represents the fault's geomorphic trace (e.g. Langridge et al., 2016; Machette et al., 2004; Styron et al., 2020). In this section, we

https://doi.org/10.5194/se-2020-104
Preprint. Discussion started: 14 July 2020



describe the methodology for mapping active faults in southern Malawi and assigning some basic geomorphological attributes. Note here that to keep the fault mapping complete for this EARS section, some faults in the SMAFD also extend into Mozambique (Fig. 2). Estimates of associated earthquake source parameters (including slip rate, earthquake magnitudes and recurrence intervals) are described in Sect. 4.

*3.1 Identifying active and inactive faults in southern Malawi*

There are many inherent limitations in mapping active faults. Even in countries with well-developed databases such as Italy and New Zealand, their success in accurately predicting the locations of future surface rupturing earthquakes is, at best, mixed (Basili et al., 2008; Nicol et al., 2016a). An active fault might not be recognised because evidence of previous surface rupture is subsequently buried, eroded (Wallace, 1980), or the fault itself is blind (e.g. Quigley et al., 2012), which in turn depends on earthquake magnitudes, thickness of the seismogenic crust, and the local geology. Furthermore, although active and inactive faults are typically differentiated by the age of the most recent earthquake, the precise maximum age that is used to define ‘active’ varies between different active fault databases depending on the regional strain rate (i.e. plate boundary vs. stable craton) and the prevalence of youthful sediments (Clark et al., 2012; Jomard et al., 2017; Langridge et al., 2016; Machette et al., 2004). Indeed, in some cases it may not be possible to reliably determine if an exposed fault has been recently ‘active’ or not (Cox et al., 2012; Nicol et al., 2016a).

Each of these issues has relevance to mapping active faults in southern Malawi. Firstly, they may be buried by sediments during regular (10-100 ka) ~100 m scale fluctuations in the level of Lake Malawi (Ivory et al., 2016; Lyons et al., 2015). Alternatively, the relatively thick (30-35 km) seismogenic crust in southern Malawi means that even moderate-large earthquakes ($M_W$>6) do not necessarily result in surface rupture, as illustrated by the $M_W$ 6.3 Salima earthquake (Gupta, 1992;

Jackson and Blenkinsop, 1993). Finally, there is little chronostratigraphic control for this section of the EARS (Dulanya, 2017; Wedmore et al., 2020a) to help differentiate between inactive and active faults.

For the SMAFD, we therefore define active faults based on evidence of activity within the current tectonic regime. Such an approach has been advocated elsewhere in the EARS (Delvaux et al., 2017) and in other areas with low levels of seismicity, few paleoseismic studies, and/or where there are faults that are favourably oriented for failure in the current stress regime, but which have no definitive evidence of recent activity (Nicol et al., 2016a; De Pascale et al., 2017; Villamor et al., 2018). In practice, this means that faults will be included in the SMAFD if they can be demonstrated to have been active during East African rifting. This evidence can vary from the accumulation of post Miocene hanging wall sediments to the presence of a steep fault scarp, offset alluvial fans, and/or knickpoints in rivers that have migrated only a short vertical distance (<100 m) upstream (Hodge et al., 2019, 2020; Jackson and Blenkinsop, 1997; Wedmore et al., 2020a). We note that the absence of post-Miocene sediments in the hanging-wall of a normal fault does not necessarily imply that it is inactive, if for example, faults are closely spaced across strike so that sediments are eroded during subsequent footwall uplift of an interior normal fault (e.g. Chirobwe-Ncheu fault, Fig. 3c; see also Mortimer et al., 2016; Muirhead et al., 2016). In these cases, if there is other evidence of recent activity (e.g. scarp, triangular facets), these faults are still included. Previous active fault mapping in southern Malawi was based on the extent of scarps alone (Hodge et al., 2019; Wedmore et al., 2020a). Therefore, the relaxed definition of an ‘active’ fault in the SMAFD means that it includes more faults than these maps, and that the lengths of some faults have been increased.

For the sake of completeness, major faults that control modern day topography, but that do not fit the criteria of being active (e.g. Karoo faults), were mapped separately (Fig. 2b). However, this map

https://doi.org/10.5194/se-2020-104
Preprint. Discussion started: 14 July 2020


is not necessarily complete for all inactive faults in southern Malawi, and we also cannot definitively exclude the possibility that some of these faults are still active although they display no evidence for it. The relatively broad definition of an active fault may also mean that some inactive faults are included in the SMAFD. However, in applying the opposite approach (i.e. requiring an absolute age for the most recent activity on a fault) there is a greater risk that faults mistakenly interpreted to be inactive subsequently rupture in a future earthquake (Litchfield et al., 2018; Nicol et al., 2016a).

### *3.2 Datasets for mapping faults in southern Malawi*

#### *3.2.1 Legacy geological maps*

Between the 1950s and 1970s, the geology of southern Malawi was systematically mapped at 1:100,000 scale and these maps, and their associated reports, were consulted in detail when defining and naming faults. These studies noted evidence of recent displacement on the Thyolo (Habgood et al., 1973), Bilila-Mtakataka, Tsikulumowa (Walshaw, 1965), and Mankanjira faults (King and Dawson, 1976). However, no attempt was made to systematically distinguish between active and inactive faults. Furthermore, there is ambiguity in these studies with equivalent structures in the Zomba Graben being variably described as 'terrace features' (Bloomfield, 1965), active fault scarps (Dixey, 1926) and Late Jurassic-Early Cretaceous faults (Dixey, 1938).

#### *3.2.2 Geophysical datasets*

Regional-scale aeromagnetic data were acquired across Malawi in 2013 by the Geological Survey Department of Malawi (Fig. 2c; Kolawole et al., 2018a; Laõ-Dávila et al., 2015). These surveys were used to refine fault mapping in cases where features interpreted as faults in the aeromagnetic survey extended beyond their surface expression. A revised fault map for the Lower Shire Graben based on gravity surveys (Chisenga et al., 2018) was also consulted when compiling the SMAFD.

https://doi.org/10.5194/se-2020-104
Preprint. Discussion started: 14 July 2020


*3.2.3 Digital Elevation Models*

The topography of southern Malawi is primarily controlled by EARS faulting (Dulanya, 2017; Laõ-Dávila et al., 2015; Wedmore et al., 2020a) except in the case of the Kirk Range (Fig. 2b), and readily identifiable igneous intrusions and Karoo faults (Figs. 3c and 4b). To exploit this interaction between topography and active faulting, TanDEM-X digital elevation models (DEMs) with a 12.5 m horizontal resolution and an absolute vertical mean error of ± 0.2 m (Wessel et al., 2018) were acquired for southern Malawi (Fig. 2b). This small error means that the TanDEM-X data performs better at identifying the metre-scale scarps common in southern Malawi (Hodge et al., 2019; Wedmore et al., 2020a) than the more widely-used but lower resolution Shuttle Radar Topography Mission (SRTM) 30 m DEMs (Sandwell et al., 2011). Furthermore, TanDEM-X data can be used to assess variations in along-strike scarp height (Hodge et al., 2018a, 2019; Wedmore et al., 2020a, 2020b) and assess the interactions between footwall uplift and fluvial incision (Fig. 4a; Wedmore et al., 2020a). The Mwanza and Nsanje faults partly extended out of the region of TanDEM-X coverage, and these sections were mapped using the SRTM 30 m resolution DEM (Fig. 2b).

*3.2.4 Fieldwork*

To corroborate evidence of recent faulting recognised in DEMs and geological reports, fieldwork was conducted on several faults (Fig. 2b). This ranged from documenting features indicative of recent displacement on the faults, such as scarps and triangular facets, to comprehensively sampling the fault and surveying it with an Unmanned Aerial Vehicle (Fig. 3; see also: Hodge et al., 2018; Wedmore et al., 2020a, 2020b; Williams et al., 2019).

*3.3 Strategy for mapping and describing active faults in the SMAFD*

Following the 'active' fault definition and synthesis of the datasets described above, faults in southern Malawi are mapped following the approach outlined for the GEM neotectonics fault

https://doi.org/10.5194/se-2020-104
Preprint. Discussion started: 14 July 2020




database (Christophersen et al., 2015; Litchfield et al., 2013). This database uses a hierarchical system to map faults, in which 'traces' are the basic unit, and one or more traces may be used to define 'sections,' and one or more sections define 'faults' (Christophersen et al., 2015; Litchfield et al., 2013). For faults in the SMAFD, which typically propagate to the surface, traces denote a linear, relatively uniform active fault geomorphic expression. The end of a trace is defined by where the geomorphic feature changes. For example, where a scarp may have been eroded to leave a gently dipping escarpment.

'Sections' are portions of faults that have a distinct geometric, kinematic, or paleoseismic attribute (Christophersen et al., 2015; Litchfield et al., 2013; Styron et al., 2020). Except in the case of linking sections, they also represent distinct surface rupturing earthquake sources in PSHA and so should be >5 km in length (Christophersen et al., 2015). Given the lack of paleoseismic information on active faults in the SMAFD, sections are generally defined by geometrical boundaries such as bends or step-overs (Fig. 2d; DuRoss et al., 2016; Jackson and White, 1989; Wesnousky, 2008; Zhang et al., 1991). Along-strike minima in fault displacement (e.g. scarp or knickpoint height) may also be indicative of segmentation (Willemse, 1997), but these do not always coincide with geometrical complexities in southern Malawi (Fig. 4; Hodge et al., 2018a, 2019; Wedmore et al., 2020a, 2020b). This may indicate that deeper structures, not visible in the surficial fault geometry, are also influencing fault segmentation (Wedmore et al., 2020b). Therefore, where along-strike scrap height measurements exist, these local minima are also used to define fault sections (Figs. 2d and 4).

'Faults' as defined by Christophersen et al. (2015) represent trace(s) and/or section(s) capable of rupturing together in a single earthquake. Empirical observations and Coulomb stress modelling suggests that normal fault earthquakes rarely rupture across steps whose width is >20% of the length

https://doi.org/10.5194/se-2020-104
Preprint. Discussion started: 14 July 2020




of the interacting sections (Biasi and Wesnousky, 2016; Hodge et al., 2018b), and we use this as a criteria to assign whether two *en echelon* sections in the SMAFD are part of the same fault.

*3.4 Fault trace attributes*

The attributes added to each mapped fault in the SMAFD are modelled on the GEM neotectonics fault database guidelines (Christophersen et al., 2015). These are listed and briefly described in Table 1, along with the hierarchical level it is assigned (i.e. trace, section, or fault). The first set of attributes is linked to information collected about each trace, and so relate to geomorphic observations (Table 1). The attributes 'scale' and 'confidence' reflect that two distinct considerations must be made when mapping a geomorphic feature as an active fault (Barrell, 2015; Styron et al., 2020): (1) its prominence in the landscape, which is indicated by the scale at which a fault is mapped, and (2) the confidence that the feature is an active fault, which indicated by a qualitative score from 1 (high) to 4 (low, Table 1).

*3.5 Section and fault geometry attributes*

The second set of attributes describes fault geometry, and these are assigned to both individual sections and whole faults (Table 1). Section length ($L_{sec}$) is defined as the straight-line distance between its end points (Fig. 4b). This approach avoids the difficulty of measuring the length of possibly fractal features, and accounts for the hypothesis that small-scale (<km scale) variations in fault geometry in southern Malawi may represent only near-surface complexity (depths <5 km), and that the faults are actually relatively planar at depth (Hodge et al., 2018a). However, it only provides a minimum estimate of section length. For segmented faults, fault length ($L_{fault}$) is the sum of $L_{sec}$, otherwise $L_{fault}$ is the distance between its tips (Fig. 4b).

https://doi.org/10.5194/se-2020-104
Preprint. Discussion started: 14 July 2020


Solid Earth Discussions

In southern Malawi, fault dip is either unknown or uncertain, because fault planes are rarely exposed, surface processes affect scarp angle (Hodge et al., 2020), and/or dip at depth is not constrained. This difficulty in measuring fault dip is commonly encountered, and in these cases dip is instead parametrised by using a range of reasonable values (Christophersen et al., 2015; Langridge et al., 2016; Styron et al., 2020). We follow this approach by assigning minimum, intermediate, and maximum dip values of 40°, 53°, and 65°, which encapsulates dip estimates from field data in southern Malawi (Hodge et al., 2018a; Williams et al., 2019), and earthquake focal mechanisms (Biggs et al., 2010; Ebinger et al., 2019), seismic reflection data (Mortimer et al., 2007; Wheeler and Rosendahl, 1994), and aeromagnetic surveys (Kolawole et al., 2018a) elsewhere in Malawi.

In the GEM neotectonics database, fault width (*W*) is estimated by projecting by the difference in lower and upper seismogenic depth into fault dip (δ), with the assumption that faults are equidimensional up to the point where *W* is limited by the thickness of the seismogenic crust (*z*; Christophersen et al., 2015):

$$W = \begin{cases} L_{fault}, & where\ L_{fault} \leq \dfrac{z}{\sin\delta}; \\ \dfrac{z}{\sin\delta}, & where\ L_{fault} > \dfrac{z}{\sin\delta} \end{cases} \tag{1}$$

In southern Malawi, both *z* (30-35 km; Jackson and Blenkinsop, 1993; Craig et al., 2011), and δ (40°-65° as justified above) are poorly constrained, so a range of *W* values must be considered. Furthermore, ruptures not limited by *z* are not necessarily equidimensional (Leonard, 2010; Wesnousky, 2008). We therefore also consider an alternative approach where *W* is estimated using an empirical scaling relationship between fault length and *W* (Leonard, 2010):

https://doi.org/10.5194/se-2020-104
Preprint. Discussion started: 14 July 2020

Solid Earth Discussions

$$W = C_1 L_{fault}^{\beta} \quad (2)$$

where $L_{fault}$ > 5km, and where $C_1$ and β are empirically derived constants and equal 17.5 and 0.66 respectively for interplate dip-slip earthquakes (Leonard, 2010).

When these equations are applied to the mapped length of faults in southern Malawi (Figs. 2 and 5a), both estimate $W$ ~ 40 km, for its longest faults ($L_{fault}$ > 50 km, Fig. 5c). Hence, Eq. 2 is consistent with observations of thick seismogneic crust in East Africa (Craig et al., 2011; Ebinger et al., 2019; Jackson and Blenkinsop, 1993; Lavayssière et al., 2019; Nyblade and Langston, 1995). However, for shorter faults ($L_{fault}$ = 5-50 km), Eq. (2) estimates smaller values of $W$ relative to the approach outlined in Eq. (1) (Fig. 5c). As noted above, this follows empirical observations that the aspect ratio of dip-slip earthquakes will be >1 where $L_{fault}$ > 5 km. In this context, Eq. (2) provides more reasonable $W$ estimates for 5-50 km long faults in south Malawi than Eq. (1) and makes little difference for longer faults; hence it is used to estimate $W$ in the SMAFD. Furthermore, along with $W$, the Leonard (2010) regressions are used to estimate earthquake magnitudes and average displacement in the SMAFD (Sect. 4.2), and so these parameters are all self-consistent.

## 4. A systems-based approach to estimating earthquake source parameters: application to the SMAFD

In addition to the active fault map, the GEM neotectonics fault database requires estimates of fault slip rates, and earthquake magnitude and recurrence intervals (Christophersen et al., 2015). However, given the lack of chronostratigraphic control for faulted surfaces in southern Malawi, no direct measurements of these attributes can be assigned to faults in the SMAFD. Indeed, as noted in the introduction, obtaining these parameters is difficult and even regions with well-developed active

https://doi.org/10.5194/se-2020-104
Preprint. Discussion started: 14 July 2020


fault databases such as in California and New Zealand only have directly measured slip rates and paleoseismic information for a small number of faults (Field et al., 2014; Langridge et al., 2016).

Instead, we suggest that fault slip rates can be estimated through a systems-level approach in which geodetically derived plate motion rates are partitioned across faults in a manner consistent with their geomorphology and regional tectonic regime. Although, such an approach has been used before over small regions (Cox et al., 2012; Litchfield et al., 2014), it has not been applied to an entire plate boundary. In addition, we also outline how the uncertainties and alternative hypotheses that are inherent to this approach can, in common with seismic hazard practice elsewhere, be explored with a logic tree approach (Fig. 6; Field et al., 2014; Vallage and Bollinger, 2019; Villamor et al., 2018).

The SMAFD is used as an example here of how this approach can be applied to a narrow amagmatic continental rift, where the distribution of regional strain between border faults and intrabasinal faults is well constrained by theoretical and observational studies (Agostini et al., 2011a; Corti, 2012; Gupta et al., 1998; Morley, 1988; Muirhead et al., 2016, 2019; Nicol et al., 1997; Shillington et al., 2020; Wedmore et al., 2020a; Wright et al., 2020). However, this framework could be adapted to other tectonic regions with well mapped active faults, few on-fault slip rate measurements, and where the partitioning of regional geodetic strain is, to an extent, predictable; for example fold and thrust belts (Koyi et al., 2000; Poblet and Lisle, 2011) and strike-slip systems (Braun and Beaumont, 1995).

*4.1 Estimating fault slip rates*

For a narrow amagmatic continental rift, the first step is to divide the rift along its axis into each of its graben/half grabens, and then within each graben/half graben, divide the mapped faults into

https://doi.org/10.5194/se-2020-104
Preprint. Discussion started: 14 July 2020




border and intrabasinal faults. Then, the slip rate for each fault or fault section *i* is estimated using the equation:

$$Slip\ rate\ (i) = \begin{cases} \dfrac{\alpha_{bf} v \cos(\theta(i) - \phi)}{n_{bf} cos\delta}, & for\ border\ faults \\ \dfrac{\alpha_{if} v \cos(\theta(i) - \phi)}{n_{if} cos\delta}, & for\ intrabasinal\ faults \end{cases} \tag{3}$$

where $\theta(i)$ is the fault or fault section slip azimuth, $v$ and $\phi$ are the horizontal rift extension rate and azimuth, $\alpha$ is a weighting applied to each fault depending on whether it is a border ($\alpha_{bf}$) or intrabasinal ($\alpha_{if}$) fault, and it is divided by the number of mapped border faults ($n_{bf}$) or intrabasinal faults ($n_{if}$) in each graben (Fig. 6). Though Eq. 3 is specific for rifts, it could be adapted in other tectonic settings, for example to distribute regional strain between the basal detachment and thrust ramps in a fold and thrust belt (Poblet and Lisle, 2011), between multiple subparallel faults in a strike-slip system, or assess more complex strain partitioning between kinematically distinct fault populations in transtensional or transpressional systems (Braun and Beaumont, 1995).

To estimate slip rates in the SMAFD we therefore first divide the rift into its principal grabens (Makanjira, Zomba, and Lower Shire, Fig. 2a). In addition, we include the Nsanje fault, which is located to the south of Malawi's principal EARS grabens (Fig. 2a) and where it bounds a poorly defined section of the EARS with low footwall relief (~300 m) and no mapped intrabasinal faults. There is, however, an eastern border fault to this section of the rift that has been mapped 25 km along strike in Mozambique (Fig. A2; Macgregor, 2015), and we group these two faults together into the same 'Nsanje' graben.

https://doi.org/10.5194/se-2020-104
Preprint. Discussion started: 14 July 2020

Solid Earth Discussions

When considering how $v$ is distributed amongst border ($\alpha_{bf}$) and intrabasinal faults ($\alpha_{if}$) in an amagmatic narrow rift, consideration should be given to factors such as total rift extension (Ebinger, 2005; Muirhead et al., 2016, 2019), rift obliquity (Agostini et al., 2011b), hanging-wall flexure (Muirhead et al., 2016; Shillington et al., 2020), lower crustal rheology (Heimpel and Olson, 1996; Wedmore et al., 2020a), and whether border faults have attained their maximum theoretical displacement (Accardo et al., 2018; Olive et al., 2014; Scholz and Contreras, 1998). As an incipient amagmatic rift, extensional strain in southern Malawi is expected to be localised (~80-90%) on its border faults (Muirhead et al., 2019; Wright et al., 2020). Furthermore, the relatively small throws on the border faults of southern Malawi (<1000 m) and thick seismogenic crust mean there that the flexural extensional strain in the hanging wall (i.e. on the intrabasinal faults) is negligible (0.1-1.2%, see Appendix A for full analysis; Billings and Kattenhorn, 2005; Muirhead et al., 2016). However, detailed analysis of fault scarp heights across the Zomba Graben indicate that ~50% of extensional strain is currently distributed onto its intrabasinal faults (Wedmore et al., 2020a). To recognise this uncertainty in the SMAFD, lower, intermediate, and upper estimates of $\alpha_{bf}$ are set to 0.5, 0.7, and 0.9 respectively, with this uncertainty explored using a logic tree (Fig. 6). Since $\alpha_{if}$ is the 'remainder' of the rift extension in each graben (i.e. $\alpha_{if} = 1 - \alpha_{bf}$), it is set to 0.1, 0.3, and 0.5 for lower, intermediate, and upper estimates (Fig. 6). For the Nsanje graben, where the rift consists of just two border faults, each fault is assigned 50% of the regional geodetic extension rate.

In the SMAFD, $v$ is taken from the plate motion vector between the Rovuma and Nubia plates at the centre of each individual graben (Table 2, Figs. 1b and A2) using the Euler poles reported in Saria et al. (2013). We use the Euler pole (as defined by a location and rotation rate) and the uncertainties associated with the Euler pole (defined by an error ellipse, Fig. B1) to calculate the plate motion and the plate motion uncertainty between the Rovuma-Nubia plates for each graben (Table 2, Fig. 1b) following the methods outlined in Robertson et al. (2016). With this approach, the lower bound of $v$

https://doi.org/10.5194/se-2020-104
Preprint. Discussion started: 14 July 2020



is negative (i.e. the plate motion is contractional, Table 2). However, the topography and seismicity of southern Malawi clearly indicate it is not a contractional regime, nor is it a stable craton. A lower bound of 0.2 mm/yr horizontal extension is therefore assigned in the SMAFD, which is considered the minimum strain accrual that is measurable using geodesy (Calais et al., 2016).

Along with uncertainty in $v$, there is also considerable uncertainty in the rift extension azimuth ($\phi$) in southern Malawi from geodesy (Table 2) due to the poorly constrained Euler pole (Saria et al., 2013). Independent measurements of regional stress and strain in southern Malawi through focal mechanism stress inversions, however, provide tighter constraints on $\phi$ (073°± 012°, Fig. 1b; Delvaux and Barth, 2010; Ebinger et al., 2019; Williams et al., 2019), and so we instead incorporate this additional prior knowledge into the SMAFD for all grabens.

As discussed in Sect. 2.3 earthquake focal mechanisms and fault slickensides in southern Malawi indicate that faults accommodate normal dip-slip motion, regardless of strike; a phenomena that can be explained by lateral heterogeneity in the lower crust (Corti et al., 2013; Philippon et al., 2015; Wedmore et al., 2020a; Williams et al., 2019). Therefore, the slip azimuth ($\theta(i)$) is equivalent to the dip direction of the fault or fault section (Fig. 6, Table 1). It is then necessary to project $\theta(i)$ into $\phi$ in Eq. (3) as these parameters are not necessarily aligned. To account for the uncertainty in $\phi$, upper and lower extension rates are obtained from varying $\phi$ by ±012° depending on the fault's dip direction (e.g. upper slip rate estimates for NE and NW dipping fault are estimated with $\phi$ set to 061° and 085° respectively, so that the difference between $\phi$ and $\theta$ tends towards 0° or 180°). In converting extension rate to fault slip rate, $\delta$ is varied between 40-65° as discussed in Sect. 3.5 (Fig. 6). Finally, unlike in the GEM neotectonic fault database, only the dip-slip rate is reported in the SMAFD as the assumption of normal faulting implies that this is equal to the net slip rate. An example of these slip rate calculations for the central section of the Chingale Step fault is provided in Fig. 7.

*4.2 Earthquake source attributes*

The next set of attributes in the GEM neotectonics fault database are related to a fault's earthquake source attributes (i.e. earthquake magnitudes and recurrence intervals, *R*; Table 1). Although these would ideally be assigned based on historical seismicity or paleoseismicity, where this information is lacking, earthquake magnitudes can by estimated using empirically derived scaling relationships between fault length and earthquake magnitude. Scaling relationships between fault length and average single event displacement ($\overline{D}$) can then be combined with slip rate estimates to calculate *R* through the relationship $R=\overline{D}$/slip rate (Cox et al., 2012; Stirling et al., 2012).

Potential errors exist in the datasets from which earthquake scaling relationships are derived, because of: (1) the possible use of inaccurate historical datasets (Stirling et al., 2013), (2) underestimates of rupture length caused by the low preservation potential of small displacement rupture tips (Hemphill-Haley and Weldon, 1999), and (3) overestimates of $\overline{D}$ from the tendency for paleoseismic investigations to target the largest scarps along a fault (DuRoss, 2008). Furthermore, in the case of southern Malawi, relatively few events from regions with thick seismogenic crust are included in these datasets, and earthquakes in such crust may follow difference scaling relationships (Hodge et al., 2020; Rodgers and Little, 2006; Smekalin et al., 2010).

To select an appropriate set of earthquake scaling relationships for the SMAFD, we consider three previously reported regressions, and apply them to its mapped faults: (1) between normal fault length and moment magnitude ($M_W$; Wesnousky, 2008), (2) interplate dip-slip fault length and $M_W$ (Leonard, 2010), and (3) fault area and $M_W$ (Wells and Coppersmith, 1994) where *A* is calculated

https://doi.org/10.5194/se-2020-104
Preprint. Discussion started: 14 July 2020



using $W$ derived from Eq. (1). Results are shown in Fig. 5d, which indicates that although generally comparable, for Mw <7.5, the Wells and Coppersmith (1994) regression overestimates magnitudes relative to Leonard (2010). This likely reflects the discrepancy in $W$ between applying Eq. (1) and the Leonard (2010) regression (Eq. (2), Fig. 5c, Sect. 3.5). The Wesnousky (2008) regression overestimates magnitudes for Mw <6.9 relative to Leonard (2010) equations and underestimates them at larger magnitudes (Fig. 5d). This may reflect that the Wesnousky (2008) regression is derived from only 6 events, and these events show a poor correlation between length and Mw (Pearson's regression coefficient = 0.36). Given the above observations, the Leonard (2010) regressions are applied to the SMAFD. Furthermore, these regressions are self-consistent when estimating Mw and $\overline{D}$, which is not necessarily true for the other cases.

We recognise that segmented normal faults may rupture in both individual sections, as demonstrated in Malawi by the Karonga earthquake sequence (Biggs et al., 2010; Fagereng, 2013), and whole fault ruptures (DuRoss et al., 2016; Goda et al., 2018; Gómez-Vasconcelos et al., 2018; Hodge et al., 2015; Iezzi et al., 2019; Valentini et al., 2020). Mw and $\overline{D}$ for each section (except linking sections) or fault $i$ in the SMAFD are therefore estimated as:

$$M_W(i) = \begin{cases} \dfrac{\left(\frac{5}{2}\log L_{sec} + \frac{3}{2}\log C_1 + \log C_2\mu\right) - 9.09}{1.5}, & for\ individual\ section\ ruptures \\ \dfrac{\left(\frac{5}{2}\log L_{fault} + \frac{3}{2}\log C_1 + \log C_2\mu\right) - 9.09}{1.5}, & for\ whole\ fault\ ruptures \end{cases} \quad (4)$$

$$\log\overline{D}(i) = \begin{cases} \frac{5}{6}\log L_{sec} + \frac{1}{2}\log C_1 + \log C_2\mu, & for\ individual\ section\ ruptures \\ \frac{5}{6}\log L_{fault} + \frac{1}{2}\log C_1 + \log C_2\mu, & for\ whole\ fault\ ruptures \end{cases} \quad (5)$$

https://doi.org/10.5194/se-2020-104
Preprint. Discussion started: 14 July 2020



where $\mu$ is the crust's shear modulus (3.3x$10^{10}$ Pa), $C_1$ is the same empirically derived constant used in Eq. (2), and $C_2$ is another constant derived by Leonard (2010). Both constants are varied between the full range of values derived in a least square analysis (Leonard, 2010) to obtain, lower, intermediate and upper estimates of $M_W$ and $\overline{D}$ (Figs. 6 and 7). Following Eq. (5), lower, intermediate, and upper estimates of each fault or section's recurrence intervals $R(i)$ can be calculated through:

$$R(i) = \frac{\overline{D}(i)}{Slip\ rate(i)} \tag{6}$$

Where upper estimates of $R$ are calculated by dividing the upper estimate of $\overline{D}$ by the lowest estimate of fault/section slip rate and vice versa (Fig. 6). An example of these earthquake source calculations for the central section of the Chingale Step fault is provided in Fig. 7.

*4.3 Miscellaneous attributes*

For each fault, a data completeness score is given, where 1 is the highest and 4 is the lowest (Table 1). This score represents the data quality of the trace, fault geometry, and slip rate attributes (Christophersen et al., 2015). In the SMAFD, the highest score is 2, given the uncertainty on fault slip rates and dip. Following the GEM template, other information for each fault includes the date of the most recent event, references for published fault mapping or derivation of fault attributes, the date that the information was last updated, the compiler of the information, and free text details recorded as 'Fault Notes' (Table 1).

https://doi.org/10.5194/se-2020-104
Preprint. Discussion started: 14 July 2020

Solid Earth Discussions

## 5. Key features of the SMAFD

### *5.1 Fault geometry, slip rates and earthquake source attributes*

Below, we present the results of applying the framework described above to faults in southern Malawi. By implementing a logic tree approach to assess uncertainty in the SMAFD, three values (lower, intermediate, and upper) are derived for each calculated attribute (Table 1, Fig. 6), with the range of values obtained by applying the lower and upper branches varying by up to three orders of magnitude. However, by using a logic tree approach, it is implicit that these upper and lower values have a low probability as they require a unique, and possibly unrealistic, combination of parameters. We therefore primarily report values obtained from applying the intermediate branches in the logic tree but discuss the uncertainties associated with our estimates in Sect. 5.3.

In total, the SMAFD contains 20 active faults, which comprise a total of 53 sections and 82 traces. Section lengths ($L_{sec}$) ranges between 6-60 km, whilst fault lengths ($L_{fault}$) varies from 11 to 150 km (Fig. 5a, Table 3). By applying Eq. (2), fault width ($W$) is typically <30 km but may exceed >40 km for the longest faults in the SMAFD (Fig. 5b, Table 3). The highest slip rates are estimated to be on the Thyolo and Zomba faults (intermediate estimates 0.6-0.8 mm/yr). On intrabasinal faults in the SMAFD, intermediate slip rate estimates are 0.05-0.1 mm/yr (Fig. 8). Slip rates tend to be relatively fast in the Makanjira Graben (Fig. 8c), as the extension rate is higher (Table 2), and its NNW-SSE striking faults are more optimally oriented to the regional extension direction (Fig. 2). The difference between upper and lower slip rate estimates in the SMAFD logic tree is two orders of magnitude; ~0.05-5 mm/yr for the border faults and ~0.005-0.5 mm/yr on the intrabasinal faults (Fig. 8).

For whole fault ruptures along border faults, intermediate estimate of earthquake recurrence intervals ($R$) are between 2000-5000 years and 10,000-30,000 years for intrabasinal whole fault ruptures (Fig. 9a-c). Considerably uncertainty exists with these values, with the upper and lower

https://doi.org/10.5194/se-2020-104
Preprint. Discussion started: 14 July 2020

Solid Earth Discussions

estimates for $R$ varying from $10^2$-$10^5$ years and ~$10^3$-$10^6$ years for border and intrabasinal whole fault ruptures respectively (Fig. 9a-c). Furthermore, if these faults rupture in individual sections, $R$ may be reduced by up to an order of magnitude (Fig. 9d-f). Intermediate estimates of earthquake magnitudes range from $M_W$ 5.4 to $M_W$ 7.2 for individual section ruptures, and $M_W$ 6.0 to $M_W$ 7.8 for faults that rupture their entire length (Table 3, Fig. 10b). Notably, we document 12 faults with the potential for hosting earthquakes greater than the largest recorded event in southern Malawi (i.e. $M_W$> 6.7, Fig. 10b, assuming intermediate branches for scaling laws in Fig. 6), the largest of which would be a $M_W$ 7.8 ± 0.5 complete rupture of the Bilila-Mtakataka or Mwanza faults.

### *5.2 Robustness of fault slip rate estimates*

The key advantage of the SMAFD in comparison to other fault maps made for the EARS (Chapola and Kaphwiyo, 1992; Delvaux et al., 2017; Macgregor, 2015) is that it provide slip rates estimates for all individual faults and fault sections (Fig. 8). It is, however, possible that some proportion of the geodetically derived rift extension may be accommodated by aseismic creep or on hitherto unrecognised faults, in which case the SMAFD estimates are effectively upper bounds. With regards to aseismic creep, the discrepancy between geodetic and seismic moment rates, and the low b-value (~0.8) for seismicity in the Karonga region implies that faults in Malawi are strongly coupled (Ebinger et al., 2019; Hodge et al., 2015). This is further supported by the velocity-weakening behaviour of samples from the rift in deformation experiments at lower crustal pressure-temperature conditions (Hellebrekers et al., 2019). We cannot definitively account for blind faults, and we recommend that future PSHA in southern Malawi should still consider 'off-fault' distributed seismic sources by using the instrumental record (e.g. Field et al., 2014; Hodge et al., 2015; Stirling et al., 2012).

https://doi.org/10.5194/se-2020-104
Preprint. Discussion started: 14 July 2020


Conversely, the possible inclusion of inactive faults in the SMAFD would mean its slip rates estimates are lower bounds. Without paleoseismic investigations and dating of faulted surfaces in southern Malawi, it is difficult to test this point. Nevertheless, reactivation analysis that encompasses the range of fault orientations in southern Malawi indicates that these faults are favourably oriented in the current stress field (Williams et al., 2019). Therefore, even faults that have been inactive for a considerable time (up to the entire age of the EARS) could still theoretically be reactivated.

An additional test for the slip rate estimates in the SMAFD is provided by comparisons to slip rates for intrabasinal faults in the North Basin of Lake Malawi. Here, Shillington et al. (2020) estimated slip rates of 0.15-0.7 mm/yr based on the 10-40 m vertical offset of a 75 ka horizon in seismic reflection data, and assuming fault dips of between 50-65°. These rates are consistent with the SMAFD only if the upper estimate branches for intrabasinal fault slip rates in the logic tree are used (Fig. 8). Alternatively, high slip rates on intrabasinal faults in northern Malawi may reflect that this section of the EARS is extending more quickly (1-3 mm/yr) as it is further from the Nubia-Rovuma Euler pole (Fig. 1a; Saria et al., 2013; Stamps et al., 2018), and/or that intrabasinal faults in southern Malawi accommodate significantly less hanging-wall flexure (0.1-1.2% vs. 2.5-7%, Appendix A; Shillington et al., 2020). In this context, the 0.05-0.1 mm/yr intermediate slip rate estimates for intrabasinal faults in the SMAFD may be consistent with these estimates in northern Malawi.

Given intermediate slip rate estimates of 0.6-0.8 mm/yr (Fig. 8) and fault dips of 53º, the throw accumulated by the border faults in the Makanjira and Zomba grabens (~350-900 m, Table A1) would have accumulated in ~0.5-1 Ma. This is younger than the estimated age for EARS rifting in central and northern Malawi (4.5-25 Ma; Delvaux, 1995; McCartney and Scholz, 2016; Mesko, 2020; Mortimer et al., 2016; Roberts et al., 2012); however, it is unclear if this indicates that the lower border fault slip rate estimates (~0.05 mm/yr) in the SMAFD should be favoured, the onset of

https://doi.org/10.5194/se-2020-104
Preprint. Discussion started: 14 July 2020



rifting occurred later in southern Malawi, or there are additional factors that have not been considered in this comparison (e.g. temporal variations in rift extension rate, footwall erosion). In either case, the range of border fault slip rate estimates in the SMAFD appears broadly consistent with age constraints for EARS rifting in southern Malawi.

*5.3 Sensitivity analysis*

Upper and lower estimates of $R$ differ by up to three orders of magnitude in the SMAFD (Fig. 9). To investigate these uncertainties, we performed a multi-parameter sensitivity analysis following the methods presented in Box et al. (1978) and Rabinowitz and Steinberg (1991). Full details of this analysis are given in Appendix B. However, in summary, 7 parameters that contribute to uncertainty in $R$ for the central section of the Chingale Step fault are considered (Table 4). By exploring all possible combinations in which these 7 parameters are set at their upper or lower estimates, 128 (i.e. $2^7$) different values of $R$ can be calculated. However, by using a fractional factorial design (Box et al., 1978), we instead considered 64 carefully selected parameter combinations at little cost to the analysis (Table B1). From these combinations, the natural log of the average value of $R$ when a parameter ($k$) is set at its upper ($\overline{\ln R}(k+)$) and lower ($\overline{\ln R}(k-)$) value is calculated and the difference between these values defines the parameter effect ($A$; Rabinowitz and Steinberg, 1991):

$$A = \overline{lnR}(k+) - \overline{lnR}(k-) \tag{7}$$

This analysis indicates that $R$ is most sensitive to uncertainties in the partitioning of strain between border and intrabasinal faults in the rift (i.e. $\alpha_{if}/n_{if}$), the rift extension rate ($v$), and the $C_2$ parameter in Eq. (5), and least sensitive to uncertainties in the rift's extension azimuth, and the $C_1$ parameter in Eq. (5) (Table 4). If, however, $v$ and its associated uncertainties were estimated using a different Nubia-Rovuma Euler pole solution (Fig. B1, Table 2; Stamps et al., 2008), $R$ estimates are least sensitive to $v$ and most sensitive to $C_2$ (Table B2). Finally, we note that there is no interaction effect between two separate parameters that may influence their sensitivity on $R$ (Table B3). These results are discussed further in Sect. 6.3

## 6. Discussion

In the following section, we examine some key results of the SMAFD in terms of its contribution to our understanding of fault growth in continental rifts, its implications for seismic hazard in southern Malawi, and future strategies to reduce its uncertainties and apply this framework to other regions.

### *6.1 Controls on fault growth in southern Malawi*

As discussed in Sect. 2.2, the height of footwall escarpments and thickness of hanging-wall sediments indicates that the rift in southern Malawi has accommodated less extension than further north in Malawi, and indeed elsewhere along the EARS (Ebinger, 1989; Muirhead et al., 2019). Nevertheless, the lengths of faults in southern Malawi (~10-150 km, Fig. 5a) are similar to lengths in more evolved sections of the EARS (Agostini et al., 2011b; Ebinger, 1989; Macgregor, 2015; Muirhead et al., 2019; Shillington et al., 2020). This suggests that faults in southern Malawi may have relatively low total displacement to length ratios. If true, this reflects the 'constant length' fault growth model (Walsh et al., 2002), with fault tip propagation potentially facilitated by exploitation of pre-existing Proterozoic fabrics that the faults follow (Fig. 2c), and which are favourably -but not optimally- oriented to the regional stresses (Williams et al., 2019).

The length scale of faults in southern Malawi also reflects its abnormally thick (30-35 km) seismogenic crust (Jackson and Blenkinsop, 1997). In particular, we document continuous 30-60 km long fault sections (Fig. 2d and 5a), whereas in typical continental crust with a 10-15 km seismogenic thickness, the length of continuous normal fault sections is typically <25 km (Jackson

https://doi.org/10.5194/se-2020-104
Preprint. Discussion started: 14 July 2020



and White, 1989). Finally, we note that though the lower crust in southern Malawi may be laterally heterogenous with localised zones of viscously deforming material (Fagereng, 2013; Hellebrekers et al., 2019; Wedmore et al., 2020a), there is geological evidence from exhumed metamorphic terranes that in dry lower crust, earthquakes may both nucleate and propagate within a predominantly viscous regime (Campbell et al., 2020; Menegon et al., 2017).

*6.2 Implications for seismic hazard in southern Malawi*

The existence of active faults within southern Malawi poses a significant risk to the 7.75 million people living in this region (Malawi National Statistics Office, 2018), and adjacent to the rift in northern Mozambique (Fig. 10a). Furthermore, with population growth at an annual rate of 2.7% in southern Malawi (Malawi National Statistics Office, 2018) this risk will increase over the coming decades. The rapidly growing city of Blantyre (population 800,000; Malawi National Statistics Office, 2018), which is in the footwall of both the relatively fast slipping (intermediate estimates ~0.8 mm/yr) Zomba and Thyolo faults is at a particularly large risk (Fig. 10a). There is therefore an urgent need to quantify the spatial and temporal distribution of this hazard through a PSHA that incorporates the earthquake source data collected in the SMAFD.

Out of a global dataset of 61 historical surface rupturing continental normal fault earthquakes, only six events had a rupture length >50 km, and only one event (the 1887 $M_W$ 7.5 Sonora earthquake) has a length >100 km (Valentini et al., 2020). Hence, the faults compiled within the SMAFD have the potential to produce the largest continental normal fault earthquake globally. However, low regional extension rates imply such events are likely to be very rare, with intermediate estimates of recurrence interval of $10^3$-$10^4$ years (Figs. 9 and 10c).

https://doi.org/10.5194/se-2020-104
Preprint. Discussion started: 14 July 2020



### *6.3 Reducing uncertainties*

#### *6.3.1. Improving fault slip rate estimates*

As noted in the introduction, one of the purposes of collating the SMAFD was to identify current knowledge gaps in our understanding of active faulting and seismic hazard in southern Malawi. Given the various aleatory (i.e. the uncertainty related to unpredictable nature of future event) and epistemic (i.e. the uncertainty due to incomplete knowledge and data) uncertainties in parameters used to derive earthquake recurrence intervals (*R*), lower and upper estimates differ by over three orders of magnitude (Fig. 9). Although such a range of estimates in a low strain rate region with limited paleoseismic information is common (e.g. Cox et al., 2012; Villamor et al., 2018) and can still be incorporated into PSHA using synthetic seismicity catalogues (Hodge et al., 2015), reducing uncertainties in these estimates in the SMAFD is an obvious priority.

Our sensitivity analysis (Sect. 5.3) indicates that the two biggest factors contributing to uncertainty in *R* in the SMAFD is related to our understanding of the distribution and rate of extension (*v*) in southern Malawi (Table 4). In particular, we note there is considerable uncertainty in the position of the Nubia-Rovuma Euler pole (Fig. B1; Saria et al., 2013), and we would not expect such large differences between upper and lower fault slip rate estimates elsewhere. Although the uncertainties associated with *v* in the SMAFD could be reduced if an alternative solution for the Nubia-Rovuma Euler pole was applied (Fig. B1, Tables 4 and B2; Stamps et al., 2008), this solution uses fewer Global Positioning System (GPS) sites and a shorter position time series (Saria et al., 2013). Furthermore, the Stamps et al. (2008) solution implies extensional rates in southern Malawi of 2.5-3 mm/yr (Table 2), which exceeds even the upper bound of those from Saria et al. (2013) model and also more recent observations of individual GPS stations in southern Malawi (1-2 mm/yr; Saria et al., 2014; Stamps et al., 2018). Therefore, in the short-term, the best refinements to *R* estimates may

https://doi.org/10.5194/se-2020-104
Preprint. Discussion started: 14 July 2020

Solid Earth Discussions

come from new regional geodetic data and further high resolution topographic analysis (e.g. Wedmore et al., 2020a).

An alternative approach to constrain *R* estimates would be to obtain on-fault slip rates and paleoseismic information in southern Malawi. However, as noted previously, this information is difficult to collect, and currently very few records exist across the entire EARS (Delvaux et al., 2017; Zielke and Strecker, 2009). Paleoseismic investigations would be particularly challenging in southern Malawi due to the potential for large (~10 m) single event displacements (Hodge et al., 2020), and that these investigations carry significant aleatory variability in low strain rate regions like southern Malawi if only a few earthquakes are sampled (Nicol et al., 2006, 2016b). This latter point reflects the fact that earthquakes may be temporally clustered in low strain rate regions (Pérouse and Wernicke, 2017; Taylor-Silva et al., 2019) due to elastic stress perturbations (Beanland and Berryman, 1989; Cowie et al., 2012; Harris, 1998; Wedmore et al., 2017); the possibility of these perturbations influencing seismicity in Malawi has already been demonstrated by the 2009 Karonga earthquake sequence (Biggs et al., 2010; Fagereng, 2013; Gaherty et al., 2019).

*6.3.2. Constraining earthquake magnitudes and fault rupture scenarios*

When considering how different rupture magnitude estimates in the SMAFD influence *R*, the main source of uncertainty is the $C_2$ parameter from the Leonard (2010) regressions (Table 4). This factor controls the amount of displacement for a given rupture area (Leonard, 2010). It is therefore likely related to stress drops, and uncertainty in $C_2$ in southern Malawi will only be reduced by recording more events in similar tectonic environments (i.e. normal fault earthquakes, ideally in regions with low (~1-10 mm/yr) extension rates and thick (20-35 km) seismogenic crust).

https://doi.org/10.5194/se-2020-104
Preprint. Discussion started: 14 July 2020



Reduced uncertainty in *R* estimates can also come from a more thorough investigation of the types (i.e. lengths) and probabilities of different rupture scenarios in the SMAFD. Notably, only end member scenarios are currently accounted for, as multi-segment ruptures that do not rupture the entire fault are not currently considered in the SMAFD. By defining faults to consist of sections capable of rupturing together in a single maximum magnitude earthquake (Christophersen et al., 2015), the rupture of multiple 'faults' is also not included. However, given events such as the 2010 El Mayor-Cucapah (Fletcher et al., 2014) and 2016 Kaikōura earthquakes (Litchfield et al., 2018) in which the rupture 'jumped' unusually large distances (>5 km), the possibility of multi-fault earthquakes in southern Malawi should not be ruled out.

Accounting for the relative probabilities of single section, multi-section, or whole fault ruptures in southern Malawi could be achieved by considering the static stress changes associated with different rupture scenarios (Parsons et al., 2012) or by generating synthetic seismic catalogues in which the relative frequency of different ruptures is fixed in a way so that the resulting magnitude-frequency distribution matches that of the instrumental earthquake catalogue (Chartier et al., 2017). Alternatively, synthetic seismicity could be generated using physics-based models (Marzocchi et al., 2009; Marzocchi and Melini, 2014; Robinson et al., 2011), which will allow a better evaluation of any earthquake clustering. Using this approach, certain branches in the logic tree used to calculate *R* (Fig. 6) could be weighted to penalise unlikely rupture scenarios. Finally, it could be recognised that the lower, intermediate, and upper estimates of *R* obtained using the SMAFD logic tree (Fig. 6) would more appropriately represented by a probability density function (e.g. Weibull, Brownian Passage Time; Pace et al., 2016), with these distributions subsequently applied when selecting *R* in a synthetic seismicity catalogue.

https://doi.org/10.5194/se-2020-104
Preprint. Discussion started: 14 July 2020



*6.4 Development of new active fault databases in other tectonic settings*

The SMAFD provides a framework for developing active fault databases within other narrow amagmatic continental rifts (e.g. Baikal Rift, Rhine Graben, Shanxi Graben). An obvious target is the extension of the SMAFD to central and northern Malawi. Here, faults under Lake Malawi, have been mapped using seismic reflection data (Flannery and Rosendahl, 1990; McCartney and Scholz, 2016; Scholz, 1989; Shillington et al., 2016, 2020), with Quaternary activity demonstrated on them by their offset of a 75 Ka horizon (Shillington et al., 2020). In addition, by combining DEMs, fieldwork, and aeromagnetic and electrical resistivity data, several onshore active faults have been documented in the region struck by the Karonga earthquake sequence (Kolawole et al., 2018b, 2018a; Macheyeki et al., 2015).

The SMAFD framework could also be applied more widely to other types of continental rifts, however, further adaptions would be required to account for blind faults in rifts with thick hanging-wall sediments, and where some component of the geodetically measured strain may be accommodated by magmatism (Bull et al., 2003; Casey et al., 2006; Ebinger, 2005; Keir et al., 2006). This framework could also be adapted for other tectonic settings with active fault maps, an *a priori* understanding of the rate and distribution of regional strain, but with few on-fault slip rate measurements; for example the Zagros fold and thrust belt (Alipoor et al., 2012; Authemayou et al., 2006; Molinaro et al., 2005) and Taiwan orogenic belt (Mouthereau et al., 2009; Shyu et al., 2016).

## 7. Conclusions

Here, we describe a new systems-based approach that combines geologic and geodetic data to estimate fault slip rates and earthquake recurrence intervals. This is then applied to faults in southern Malawi, which has led to the development of the South Malawi Active Fault Database (SMAFD), a geospatial database designed to direct future research and aid seismic hazard assessment and

https://doi.org/10.5194/se-2020-104
Preprint. Discussion started: 14 July 2020



planning. The SMAFD reveals that active faults with the potential for $M_W > 7$ earthquakes exist across southern Malawi. That earthquakes of such magnitude can occur within this incipient section of the East African Rift System (EARS) reflects a combination of thick (30-35 km) seismogenic crust and fault lengthening that may have been facilitated by the exploitation of favourably oriented pre-existing crustal weaknesses.

Slow geodetically-derived extension rates (~1 mm/yr) imply that the faults themselves have low slip rates (0.001-5 mm/yr), and so the recurrence intervals of $M_W > 7$ events are estimated to be on the order of $10^2$-$10^6$ years. The large range of these estimated recurrence times reflects aleatory uncertainty on fault rupture scenarios and epistemic uncertainties in fault-scaling relationships, fault slip rates, and fault geometry. Sensitivity analysis suggests the biggest reduction in uncertainties would come from improved knowledge of fault slip rates through paleoseismic investigations or geodetic studies. Nevertheless, the combination of long, highly-coupled, low slip rate faults and a short (<65 years) instrumental record imply that the SMAFD is an important source of information for future seismic hazard assessments within the rift. In this respect, the development of SMAFD is timely as the seismic risk of southern Malawi is growing due to rapid population growth. urbanisation, and seismically vulnerable building stock. Similar challenges exist elsewhere along the EARS, which may also be partially addressed by following the framework provided by SMAFD.

## Appendices

### Appendix A: Hanging-wall flexure in southern Malawi

The considerable amounts of throw (>1000 m) along a rift bounding fault can induce a significant amount of flexure within the lithosphere either side of the fault (Muirhead et al., 2016; Olive et al., 2014; Petit and Ebinger, 2000; Shillington et al., 2020). In the case of the hanging-wall, this is a

https://doi.org/10.5194/se-2020-104
Preprint. Discussion started: 14 July 2020



downward flexure that can result in intrabasinal faults accommodating additional slip to that imparted by regional extension alone (Muirhead et al., 2016). This additional flexural strain must therefore be accounted for when considering the distribution of strain in southern Malawi.

Here, strain due to hanging-wall flexure is estimated in profiles across southern Malawi using the methodology described by Muirhead et al. (2016), which is based on the equations presented in Turcotte and Schubert (1982) and Billings and Kattenhorn (2005). These flexural profiles are also compared to those made for the North Basin of Lake Malawi using the same method (Shillington et al., 2020). This method calculates flexure by considering a vertical line-load at the point of maximum deflection (i.e. at the upper contact of the border fault hanging wall, Fig. A1). The deflection (ω) across a border fault hanging wall can then be estimated as:

$$\omega = \omega_0 e^{\frac{-x}{\alpha}} \cos\left(\frac{x}{\alpha}\right) \tag{A1}$$

where $\omega_0$ is the maximum deflection, $x$ is the position along a hanging wall profile from the deflecting fault (Fig. A1), and α is:

$$\alpha = \left[\frac{E h^3}{\left(3\rho_0 g(1-v^2)\right)}\right]^{\frac{1}{4}} \tag{A2}$$

where $E$ is Young's Modulus, $v$ is Poisson's ratio (0.25), $g$ is acceleration due to gravity (9.8 m/s$^2$), $h$ is the thickness of elastic crust, which is assumed here to be the equivalent to the thickness of the seismogenic crust (30-35 km, Fig. A1; Jackson and Blenkinsop, 1993; Craig et al., 2011; Ebinger et al., 2019), and $\rho_0$ is crustal density, for which the average crustal density (2816 kg/m$^3$) for the Malawi Rift from a three layer model is used (Fagereng, 2013; Nyblade and Langston, 1995). In this

https://doi.org/10.5194/se-2020-104
Preprint. Discussion started: 14 July 2020

Solid Earth Discussions

analysis, a value of $E$, such that the hanging wall deflection is restricted to a distance comparable to the actual width of the half-graben is used (Muirhead et al., 2016; Shillington et al., 2020). Using this principle, a comparatively low value of $E$ (3 GPa) is required to fit the flexure profiles across southern Malawi's ~50 km wide half-grabens, although this is comparable to $E$ used during similar analysis elsewhere in the East African Rift System (EARS; Muirhead et al., 2016; Shillington et al., 2020).

In Eq. A1, $\omega_0$ can be derived through the observation from real and modelled normal faults that the ratio ($r$) of upthrow to downthrow along a normal fault is typically 0.2 (Muirhead et al., 2016). Therefore:

$$\omega_0 = BF_{throw}(1 - r) \tag{A3}$$

Where $BF_{throw}$ is border fault throw and is equivalent to the sum of the footwall escarpment height and hanging wall sediment thickness. There are significant uncertainties in estimating sediment thickness within southern Malawi, hence a range of values are used (Table A1). Uncertainty is highest in the Lower Shire Graben where no boreholes have penetrated basement (Habgood et al., 1973), and where the contribution of Karoo rifting to hanging wall flexure of the Thyolo Fault also needs to be considered (Castaing, 1991; Chisenga et al., 2018). Castaing (1991) report throws of 1000 m for other Karoo faults in the Lower Shire Graben, and that the Thyolo Fault would have been in transtension during the main Permian to Lower Jurassic period of Karoo extension. Furthermore, given the overall southward propagation of the EARS (Ebinger, 1989), it is unlikely that it would have accommodated more throw than the border faults in the Zomba and Makanjira grabens (~1000 m, Table A1) during this phase of rifting. Therefore, it is unlikely that total throw

https://doi.org/10.5194/se-2020-104
Preprint. Discussion started: 14 July 2020



along the Thyolo Fault exceeds 2000 m. As a full graben, we consider the hanging-wall flexure across both sides of the Makanjira Graben (Fig. A2).

Given a profile of hanging wall deflection, it is possible to derive the resulting flexural extensional strain (ε) within a half-graben (Billings and Kattenhorn, 2005; Muirhead et al., 2016):

$$\varepsilon = -y\left(\frac{d^2\omega}{dx^2}\right) \tag{A4}$$

where $y$ is the vertical distance from the centre of the plate (downward is positive, Fig. A1). The Zomba and Lower Shire grabens are ~50 km wide (Fig. A2), therefore the mean flexural strain over this distance is reported. For the Makanjira graben, we calculate the mean strain from the contribution of each side of the graben over its 75 km width. From these values, the magnitude of flexural horizontal extension over each graben is calculated, as is the extension rate (both rift wide, and per fault average) assuming a range of graben ages (McCartney and Scholz, 2016; Roberts et al., 2012). In calculating flexural extension rates for the Lower Shire Graben, we assume that 50% of the flexure in this graben is a result of Karoo rifting, and so calculate rates of EARS flexure based on half of the strain values reported in Table A1.

Results of this analysis are shown in Fig. A3 and Table A1. These demonstrate that regardless of the simplifications, uncertainties and assumptions in this analysis, hanging-wall flexure in southern Malawi is negligible (strains <1%, slip rates due to hanging-wall flexure <0.03 mm/yr per fault). This reflects the thick seismogenic crust in southern Malawi (e.g. Craig et al., 2011) and relatively small amounts of throw across its border faults (<2000 m). For example, when compared to border faults in northern Malawi (throw ~7000 m; Accardo et al., 2018), the magnitude of hanging-wall flexure is considerably larger (strains 2-7%, Table A1, Shillington et al., 2020) . We therefore do not

https://doi.org/10.5194/se-2020-104
Preprint. Discussion started: 14 July 2020


consider hanging-wall flexure further when considering the slip rate of intrabasinal faults in southern Malawi (Sect. 4.1, main text).

**Appendix B: A multiparameter sensitivity analysis for recurrence interval estimates in the South Malawi Active Fault Database**

Recurrence interval estimates in the South Malawi Active Fault Database (SMAFD) vary by over three orders of magnitude (Fig. 9). These uncertainties are not unexpected in a region like Malawi with no paleoseismic data and an incomplete instrumental seismic record (Cox et al., 2012; Villamor et al., 2018), and can be accounted for in Probabilistic Seismic Hazard Assessment (PSHA) using synthetic seismicity catalogues (Hodge et al., 2015). Nevertheless, by conducting a sensitivity analysis on the logic tree approach used to calculate these recurrence intervals (Fig. 6), it is possible to determine which parameters contribute most to this uncertainty, and therefore guide future research directions that will help constrain them in future iterations of the SMAFD. This analysis is briefly described in the main text (Sect. 5.3, Table 4), and is documented fully below.

Here, we follow the multiparameter sensitivity analysis presented by Rabinowitz and Steinberg (1991). This study conducted sensitivity analysis for the parameters that feed into PSHA, where the output metric is the probability of exceedance of a given level of ground shaken. For the SMAFD, we adapt this method to test the sensitivity of seven parameters that are used to calculate earthquake recurrence intervals (*R*, Eq. B1, Table 4). This metric is chosen as it fully incorporates the aleatory uncertainties in rupture length, and epistemic uncertainties in fault slip rates and the Leonard (2010) scaling relationships (Fig. 6). This analysis is performed for the Chingale Step fault central section (Fig. 4), where like all intrabasinal faults in the SMAFD, *R* is calculated by:

https://doi.org/10.5194/se-2020-104
Preprint. Discussion started: 14 July 2020


$$R = \frac{\left(\frac{5}{6}logL + \frac{1}{2}logC_1 + logC_2\right)\left(n_{if}cos\delta\right)}{\alpha_{if}vcos(\theta - \phi)} \tag{B1}$$

Where $L$ is rupture length and depends on whether an individual section ($L_{sec}$) or whole fault ($L_{fault}$) rupture is considered, $C_1$ and $C_2$ are empirically derived constants from Leonard (2010), $\delta$ is fault dip, $\theta$ is the fault slip azimuth, $v$ and $\phi$ are the rift extension rate and azimuth, $\alpha_{if}$ is a weighting of rift extension for intrabasinal faults, and $n_{if}$ is the number of mapped intrabasinal faults ($n_{if}$) in the graben.

Eq. B1 is essentially a combination of Eqs. 3, 5, and 6 in the main text, and its application with the SMAFD logic tree to calculate $R$ for the Chingale Step fault central section is shown in Fig. 7. There are 5 intrabasinal faults in the Zomba Graben where the Chingale Step fault is situated (Fig. 2), and in this analysis, this parameter is not treated as an uncertainty. However, for simplicity, it is combined with $\alpha_{if}$ to give the 'component of rift extensional strain' parameter, which is defined by $\alpha_{if}/n_{if}$ (Table 4). Assuming that the Chingale Step fault is a normal fault (Wedmore et al., 2020a; Williams et al., 2019), $\theta$ is the fault dip direction, and differs by only 4° depending on whether the whole fault ruptures or just the central section (Fig. 7). Hence uncertainity in this parameter is not considered here, and it is set at 290°, which is the average value for these two rupture scenarios. When assessing the influence of $v$, we consider two geodetic models (Fig. B1; Saria et al., 2013; Stamps et al., 2008), and perform this sensitivity analysis for both.

The method presented by Rabinowitz and Steinberg (1991) involves a two-level fractional factorial multiparameter design, where each parameter is restricted to the two levels which will give lower or upper estimates of $R$ (Table 4). Ideally, these levels would be symmetric about the intermediate case, however, in the SMAFD this is not possible for the $v$, $L$, and $C_2$. Compared to a 'one at-a-time

https://doi.org/10.5194/se-2020-104
Preprint. Discussion started: 14 July 2020


(OAT)' parameter analysis, a multiparameter analysis allows us to assess how different parameters interact with each other, and so more fully explore the parameter space (Rabinowitz and Steinberg, 1991). This is achieved through a factorial design, which for the seven parameters ($k$) tested here would generate 128 (i.e. $2^{7}$) possible combinations in a full two-level factorial approach. However, in a fractional factorial design, just a subset of these combinations is assessed. This approach recognises that many of the combinations in a full factorial design offer little insight into how a system works, and that this can instead be achieved at minimal cost to the results by considering a carefully selected subset of these combinations (Box et al., 1978; Rabinowitz and Steinberg, 1991). In this analysis, $2^{k-p}$ combinations are assessed where $p$ is the number of generators and is set at 1. This results in the assessment of 64 combinations (Table B1) and a 'resolution' of 5, which means it is possible to estimate the main effects of each parameter (Eq. B2), interactions between two parameters (Eq. B3), but not interactions between three parameters (Box et al., 1978).

The main effect ($A$) of one parameter (e.g. fault dip, δ) is quantified from the difference between the average of the natural log of recurrence interval ($\overline{\ln R}$) for the 32 combinations in Table B1 when a parameter was at its upper level (i.e. δ+ = 40°) and $\overline{\ln R}$ for the 32 combinations when the parameter was at its low level (i.e. δ- = 65°):

$$A = \overline{lnR}(\delta +) - \overline{lnR}(\delta -) \tag{B2}$$

By applying a multiparameter approach it is also possible to the quantify parameter-parameter interaction effects, for example, if the effect of δ depends on the choice of rift extension azimuth (ϕ). To do this, the results in Table B1 can be divided into two sets with $2^{k-p-1}$ combinations each depending on which level of δ was applied. Following the table designs developed by Box et al. (1978), each set of 32 combinations will have 16 combinations when ϕ was at is upper level (ϕ+)

https://doi.org/10.5194/se-2020-104
Preprint. Discussion started: 14 July 2020



and 16 combinations when ϕ was at its lower level (ϕ-). The effect of δ on each level of ϕ (i.e. δϕ) is then calculated from the corresponding averages differences in $\overline{\ln R}$ (Rabinowitz and Steinberg, 1991):

$$\delta\phi = \left(\overline{lnR}(\delta + \phi +) - \overline{lnR}(\delta - \phi +)\right) - \left(ln\bar{R}(\delta + \phi -) - \overline{lnR}(\delta - \phi -)\right) \quad \text{(B3)}$$

If there is no interaction effect between these two parameters, then δϕ is 0. Otherwise, the size of the effect is proportional to the magnitude of δϕ. In addition, we demonstrate our results in terms of an empirical cumulative distribution function for the values of ln*R* reported in Table B1 (Fig. B2a), and following Rabinowitz and Steinberg (1991), values of *A* in a normal probability plot (Fig. B1b).

If the Saria et al. (2013) model is used to provide estimates of *v* in this sensitivity analysis, the parameter that contributes most to uncertainties of *R* in the SMAFD is the component of regional extensional strain that each fault accommodates (A = 3.05, Table 4). This essentially means that ln*R* is higher by 3.05 when this component is set at its high value compared to its lower, or that *R* is ~21 times ($e^{3.05}$) higher when 10% of regional extensional strain is assigned to the Chingale Step fault as opposed to 2%. The importance of this parameter is also demonstrated by the fact that it does not plot close to the normal distribution line in Fig. B1b. The parameters with the next highest main effect on *R* are *v* and $C_2$, whilst estimates of *R* are least sensitive to uncertainties in ϕ (Table 4). If, however, estimates of *v* are provided by the Stamps et al. (2008) model (Fig. B1), estimates of *R* are considerably less sensitive to uncertainites in rift extension rates, and the $C_2$ parameter has the biggest influence on *R* (Table B2). Multiparameter effects are all equal to zero (Table B3) regardless of geodetic model, and thus the sensitivity of each of these parameters is independent of changes in other parameters.

https://doi.org/10.5194/se-2020-104
Preprint. Discussion started: 14 July 2020



The results of the sensitivity analysis reported here are specific to estimates of *R* for the Chingale Step fault central section, however, results should be broadly applicable to all other faults in the SMAFD as *R* was calculated following the same steps. There will, however, be differences for faults that are not segmented (where *L* is not an uncertainty) or that have more than the three sections mapped along the Chingale Step fault (e.g. the seven section Bilila-Mtakataka). The uncertainty in the weighting of rift extension may also be different for border faults, as in these cases the weighting factor ($\alpha_{bf}$) is varied between 0.5-0.9. The results of this analysis are discussed further in Sect. 5.3 and 6.3 in the main text.

**Data Availability**

The South Malawi Active Fault Database is available in the Supplement as a Shapefile.

**Author Contributions**

JW and LW led the fault mapping from TanDEM-X data, and HM led the fault mapping using aeromagnetic data. All authors participated in the fieldwork. LW conducted analysis of geodetic data. JW designed the method to obtain fault slip rates and earthquake source parameters with input from all co-authors. JB and AF secured the funding for this project. All authors contributed to manuscript preparation, but JW had primary responsibility.

**Competing interests**

The authors declare that they have no conflict of interest.

**Acknowledgements**

This work is supported by the EPSRC-Global Challenges Research Fund PREPARE project (EP/P028233/1). TanDEM-X data were provided through DLR proposal DEM_GEOL0686. The Geological Survey Department of Malawi kindly gave us access to the 2013 aeromagnetic surveys across Malawi. We thank Katsu Goda and Mark Stirling for useful discussions on developing this

https://doi.org/10.5194/se-2020-104
Preprint. Discussion started: 14 July 2020


database, and Mike Floyd for his assistance with calculating geodetic extension rates from Euler Poles.

https://doi.org/10.5194/se-2020-104
Preprint. Discussion started: 14 July 2020



**References**

Accardo, N. J., Shillington, D. J., Gaherty, J. B., Scholz, C. A., Nyblade, A. A., Chindandali, P. R. N., Kamihanda, G., McCartney, T., Wood, D. and Wambura Ferdinand, R.: Constraints on Rift Basin Structure and Border Fault Growth in the Northern Malawi Rift From 3-D Seismic Refraction Imaging, J. Geophys. Res. Solid Earth, 123(11), 10,003-10,025, doi:10.1029/2018JB016504, 2018.

Agostini, A., Bonini, M., Corti, G., Sani, F. and Manetti, P.: Distribution of Quaternary deformation in the central Main Ethiopian Rift, East Africa, Tectonics, 30(4), doi:10.1029/2010TC002833, 2011a.

Agostini, A., Bonini, M., Corti, G., Sani, F. and Mazzarini, F.: Fault architecture in the Main Ethiopian Rift and comparison with experimental models: Implications for rift evolution and Nubia-Somalia kinematics, Earth Planet. Sci. Lett., 301(3–4), 479–492, doi:10.1016/j.epsl.2010.11.024, 2011b.

Alipoor, R., Zaré, M. and Ghassemi, M. R.: Inception of activity and slip rate on the Main Recent Fault of Zagros Mountains, Iran, Geomorphology, 175–176, 86–97, doi:10.1016/j.geomorph.2012.06.025, 2012.

Ambraseys, N. N.: The Rukuwa Earthquake of 13 December 1910 In East-Africa, Terra Nov., 3(2), 202–211, doi:10.1111/j.1365-3121.1991.tb00873.x, 1991.

Andreoli, M. A. G.: Petrochemistry, tectonic evolution and metasomatic mineralisations of Mozambique belt granulites from S Malawi and Tete (Mozambique), Precambrian Res., 25(1–3), 161–186, doi:10.1016/0301-9268(84)90031-7, 1984.

Authemayou, C., Chardon, D., Bellier, O., Malekzadeh, Z., Shabanian, E. and Abbassi, M. R.: Late Cenozoic partitioning of oblique plate convergence in the Zagros fold-and-thrust belt (Iran), Tectonics, 25(3), doi:10.1029/2005TC001860, 2006.

https://doi.org/10.5194/se-2020-104
Preprint. Discussion started: 14 July 2020


Ayele, A.: Probabilistic seismic hazard analysis (PSHA) for Ethiopia and the neighboring region, J. African Earth Sci., 134, 257–264, doi:10.1016/j.jafrearsci.2017.06.016, 2017.

Barrell, D. J. A.: General distribution and characteristics of active faults and folds in the Kaikoura District, North Canterbury, GNS Science Consultancy Report 2014/210; Environment Canterbury Report R15/23. Christchurch, New Zealand; Environment Canterbury Regional Council., 2015.

Basili, R., Valensise, G., Vannoli, P., Burrato, P., Fracassi, U., Mariano, S., Tiberti, M. M. and Boschi, E.: The Database of Individual Seismogenic Sources (DISS), version 3: Summarizing 20 years of research on Italy's earthquake geology, Tectonophysics, 453(1–4), 20–43, doi:10.1016/j.tecto.2007.04.014, 2008.

Beanland, S. and Berryman, K. R.: Style and episodicity of late quaternary activity on the pisa-grandview fault zone, Central Otago, New Zealand, New Zeal. J. Geol. Geophys., 32(4), 451–461, doi:10.1080/00288306.1989.10427553, 1989.

Beauval, C., Marinière, J., Yepes, H., Audin, L., Nocquet, J. M., Alvarado, A., Baize, S., Aguilar, J., Singaucho, J. C. and Jomard, H.: A new seismic hazard model for ecuador, Bull. Seismol. Soc. Am., 108(3), 1443–1464, doi:10.1785/0120170259, 2018.

Biasi, G. P. and Wesnousky, S. G.: Steps and gaps in ground ruptures: Empirical bounds on rupture propagation, Bull. Seismol. Soc. Am., 106(3), 1110–1124, doi:10.1785/0120150175, 2016.

Biggs, J., Nissen, E., Craig, T., Jackson, J. and Robinson, D. P.: Breaking up the hanging wall of a rift-border fault: The 2009 Karonga earthquakes, Malawi, Geophys. Res. Lett., 37(11), doi:10.1029/2010GL043179, 2010.

Billings, S. E. and Kattenhorn, S. A.: The great thickness debate: Ice shell thickness models for Europa and comparisons with estimates based on flexure at ridges, Icarus, 177(2), 397–412, doi:10.1016/j.icarus.2005.03.013, 2005.

https://doi.org/10.5194/se-2020-104
Preprint. Discussion started: 14 July 2020


Bloomfield, K.: The geology of the Port Herald Area, Bull. Geol. Surv. Malawi, 9, 1958.

Bloomfield, K.: The Geology of the Zomba Area, Bull. Geol. Surv. Malawi, 16, 1965.

Bloomfield, K. and Garson, M. S.: The Geology of the Kirk Range-Lisungwe Valley Area, Bull. Geol. Surv. Malawi, 17, 1965a.

Bloomfield, K. and Garson, M. S.: The Geology of the Kirk Range-Lisungwe Valley Area, Bull. Geol. Soc. Am., 17, 1965b.

Box, G. E. P., Hunter, W. G. and Hunter, J. S.: Statistics for experimenters, John Wiley and sons New York., 1978.

Brace, W. F. and Byerlee, J. D.: Stick-slip as a mechanism for earthquakes, Science (80-. )., 153(3739), 990–992, 1966.

Braun, J. and Beaumont, C.: Three-dimensional numerical experiments of strain partitioning at oblique plate boundaries: implications for contrasting tectonic styles in the southern Coast Ranges, California, and central South Island, New Zealand, J. Geophys. Res., 100(B9), doi:10.1029/95jb01683, 1995.

De Bremaeker, J.-C.: Premières données séismologiques sur le Graben de l'Afrique Centrale. Acad. R. Sci. Coloniales, Bull. II-1956, 4, 762–787, 1956.

Buck, W. R.: Modes of continental lithospheric extension, J. Geophys. Res., 96(B12), doi:10.1029/91jb01485, 1991.

Bull, J. M., Minshull, T. A., Mitchell, N. C., Thors, K., Dix, J. K. and Best, A. I.: Fault and magmatic interaction within Iceland's western rift over the last 9 kyr, Geophys. J. Int., 154(1), F1–F8, doi:10.1046/j.1365-246X.2003.01990.x, 2003.

Calais, E., Camelbeeck, T., Stein, S., Liu, M. and Craig, T. J.: A new paradigm for large earthquakes

https://doi.org/10.5194/se-2020-104
Preprint. Discussion started: 14 July 2020



in stable continental plate interiors, Geophys. Res. Lett., 43(20), 10,621-10,637, doi:10.1002/2016GL070815, 2016.

Campbell, L. R., Menegon, L., Fagereng, Å. and Pennacchioni, G.: Earthquake nucleation in the lower crust by local stress amplification, Nat. Commun., 11(1), 1–9, 2020.

Casey, M., Ebinger, C. J., Keir, D., Gloaguen, R. and Mohamed, F.: Strain accommodation in transitional rifts: extension by magma intrusion and faulting in Ethiopian rift magmatic segments, Geol. Soc. Spec. Publ., 259, 143–163, doi:10.1144/GSL.SP.2006.259.01.13, 2006.

Castaing, C.: Post-Pan-African tectonic evolution of South Malawi in relation to the Karroo and recent East African rift systems, Tectonophysics, 191(1–2), 55–73, doi:10.1016/0040-1951(91)90232-H, 1991.

Chapola, L. S. and Kaphwiyo, C. E.: The Malawi rift: Geology, tectonics and seismicity, Tectonophysics, 209(1–4), 159–164, doi:10.1016/0040-1951(92)90017-Z, 1992.

Chartier, T., Scotti, O., Lyon-Caen, H. and Boiselet, A.: Methodology for earthquake rupture rate estimates of fault networks: Example for the western Corinth rift, Greece, Nat. Hazards Earth Syst. Sci., 17, 1857–1869, doi:10.5194/nhess-17-1857-2017, 2017.

Chisenga, C., Dulanya, Z. and Jianguo, Y.: The structural re-interpretation of the Lower Shire Basin in the Southern Malawi rift using gravity data, J. African Earth Sci., (September), 1–11, doi:10.1016/j.jafrearsci.2018.08.013, 2018.

Christophersen, A., Litchfield, N., Berryman, K., Thomas, R., Basili, R., Wallace, L., Ries, W., Hayes, G. P., Haller, K. M., Yoshioka, T., Koehler, R. D., Clark, D., Wolfson-Schwehr, M., Boettcher, M. S., Villamor, P., Horspool, N., Ornthammarath, T., Zuñiga, R., Langridge, R. M., Stirling, M. W., Goded, T., Costa, C. and Yeats, R.: Development of the Global Earthquake Model's neotectonic fault database, Nat. Hazards, 79(1), 111–135, doi:10.1007/s11069-015-1831-6, 2015.

Clark, D., McPherson, A. and Van Dissen, R.: Long-term behaviour of Australian stable continental region (SCR) faults, Tectonophysics, 566–567, 1–30, doi:10.1016/j.tecto.2012.07.004, 2012.

Corti, G.: Evolution and characteristics of continental rifting: Analog modeling-inspired view and comparison with examples from the East African Rift System, Tectonophysics, 522–523(1), 1–33, doi:10.1016/j.tecto.2011.06.010, 2012.

Corti, G., Philippon, M., Sani, F., Keir, D. and Kidane, T.: Re-orientation of the extension direction and pure extensional faulting at oblique rift margins: Comparison between the Main Ethiopian Rift and laboratory experiments, Terra Nov., 25(5), 396–404, doi:10.1111/ter.12049, 2013.

Cowie, P. A., Roberts, G. P., Bull, J. M. and Visini, F.: Relationships between fault geometry, slip rate variability and earthquake recurrence in extensional settings, Geophys. J. Int., 189(1), 143–160, doi:10.1111/j.1365-246X.2012.05378.x, 2012.

Cox, S. C., Stirling, M. W., Herman, F., Gerstenberger, M. and Ristau, J.: Potentially active faults in the rapidly eroding landscape adjacent to the Alpine Fault, central Southern Alps, New Zealand, Tectonics, 31(2), doi:10.1029/2011TC003038, 2012.

Craig, T. J., Jackson, J. A., Priestley, K. and Mckenzie, D.: Earthquake distribution patterns in Africa: Their relationship to variations in lithospheric and geological structure, and their rheological implications, Geophys. J. Int., 185(1), 403–434, doi:10.1111/j.1365-246X.2011.04950.x, 2011.

Delvaux, D.: Age of Lake Malawi (Nyasa) and water level fluctuations, Mus. roy. Afrr. centr., Tervuren (Belg.), Dept. Geol. Min., Rapp. ann. 1993 1994, 108, 99–108, 1995.

Delvaux, D. and Barth, A.: African stress pattern from formal inversion of focal mechanism data, Tectonophysics, 482(1–4), 105–128, doi:10.1016/j.tecto.2009.05.009, 2010.

Delvaux, D., Mulumba, J. L., Sebagenzi, M. N. S., Bondo, S. F., Kervyn, F. and Havenith, H. B.:

https://doi.org/10.5194/se-2020-104
Preprint. Discussion started: 14 July 2020


Seismic hazard assessment of the Kivu rift segment based on a new seismotectonic zonation model (western branch, East African Rift system), J. African Earth Sci., 134, 831–855, doi:10.1016/j.jafrearsci.2016.10.004, 2017.

Dixey, F.: The Nyasaland section of the great rift valley, Geogr. J., 68(2), 117–137, 1926.

Dixey, F.: The Nyasa-Shire Rift, Geogr. J., 91(1), 51–56, 1938.

Dulanya, Z.: A review of the geomorphotectonic evolution of the south Malawi rift, J. African Earth Sci., 129, 728–738, doi:10.1016/j.jafrearsci.2017.02.016, 2017.

Dulanya, Z., Morales-Simfors, N. and Sivertun, Å.: Comparative study of the silica and cation geothermometry of the Malawi hot springs: Potential alternative energy source, J. African Earth Sci., 57(4), 321–327, doi:10.1016/j.jafrearsci.2009.11.001, 2010.

DuRoss, C. B.: Holocene vertical displacement on the central segments of the Wasatch fault zone, Utah, Bull. Seismol. Soc. Am., 98(6), 2918–2933, doi:10.1785/0120080119, 2008.

DuRoss, C. B., Personius, S. F., Crone, A. J., Olig, S. S., Hylland, M. D., Lund, W. R. and Schwartz, D. P.: Fault segmentation: New concepts from the Wasatch Fault Zone, Utah, USA, J. Geophys. Res. Solid Earth, 121(2), 1131–1157, doi:10.1002/2015JB012519, 2016.

Ebinger, C.: Continental break-up: The East African perspective, Astron. Geophys., 46(2), 2.16-2.21, doi:10.1111/j.1468-4004.2005.46216.x, 2005.

Ebinger, C. J.: Tectonic development of the western branch of the East African rift system, Geol. Soc. Am. Bull., 101(7), 885–903, doi:10.1130/0016-7606(1989)101<0885:TDOTWB>2.3.CO;2, 1989.

Ebinger, C. J., Rosendahl, B. R. and Reynolds, D. J.: Tectonic model of the Malaŵi rift, Africa, Tectonophysics, 141(1–3), 215–235, doi:10.1016/0040-1951(87)90187-9, 1987.

https://doi.org/10.5194/se-2020-104
Preprint. Discussion started: 14 July 2020


Ebinger, C. J., Oliva, S. J., Pham, T. Q., Peterson, K., Chindandali, P., Illsley-Kemp, F., Drooff, C., Shillington, D. J., Accardo, N. J., Gallacher, R. J., Gaherty, J., Nyblade, A. A. and Mulibo, G.: Kinematics of Active Deformation in the Malawi Rift and Rungwe Volcanic Province, Africa, Geochemistry, Geophys. Geosystems, 20(8), 3928–3951, doi:10.1029/2019GC008354, 2019.

Eby, G. N., Roden-Tice, M., Krueger, H. L., Ewing, W., Faxon, E. H. and Woolley, A. R.: Geochronology and cooling history of the northern part of the Chilwa Alkaline Province, Malawi, J. African Earth Sci., 20(3–4), 275–288, doi:10.1016/0899-5362(95)00054-W, 1995.

Fagereng, Å.: Fault segmentation, deep rift earthquakes and crustal rheology: Insights from the 2009 Karonga sequence and seismicity in the Rukwa-Malawi rift zone, Tectonophysics, 601, 216–225, doi:10.1016/j.tecto.2013.05.012, 2013.

Field, E. H., Arrowsmith, R. J., Biasi, G. P., Bird, P., Dawson, T. E., Felzer, K. R., Jackson, D. D., Johnson, K. M., Jordan, T. H. and Madden, C.: Uniform California earthquake rupture forecast, version 3 (UCERF3)—The time-independent model, Bull. Seismol. Soc. Am., 104(3), 1122–1180, 2014.

Flannery, J. W. and Rosendahl, B. R.: The seismic stratigraphy of Lake Malawi, Africa: implications for interpreting geological processes in lacustrine rifts, J. African Earth Sci., 10(3), 519–548, doi:10.1016/0899-5362(90)90104-M, 1990.

Fletcher, J. M., Teran, O. J., Rockwell, T. K., Oskin, M. E., Hudnut, K. W., Mueller, K. J., Spelz, R. M., Akciz, S. O., Masana, E., Faneros, G., Fielding, E. J., Leprince, S., Morelan, A. E., Stock, J., Lynch, D. K., Elliott, A. J., Gold, P., Liu-Zeng, J., González-Ortega, A., Hinojosa-Corona, A. and González-García, J.: Assembly of a large earthquake from a complex fault system: Surface rupture kinematics of the 4 April 2010 El Mayor-Cucapah (Mexico) M w 7.2 earthquake, Geosphere, 10(4), 797–827, doi:10.1130/GES00933.1, 2014.

https://doi.org/10.5194/se-2020-104
Preprint. Discussion started: 14 July 2020


Fritz, H., Abdelsalam, M., Ali, K. A., Bingen, B., Collins, A. S., Fowler, A. R., Ghebreab, W., Hauzenberger, C. A., Johnson, P. R., Kusky, T. M., Macey, P., Muhongo, S., Stern, R. J. and Viola, G.: Orogen styles in the East African Orogen: A review of the Neoproterozoic to Cambrian tectonic evolution, J. African Earth Sci., 86, 65–106, doi:10.1016/j.jafrearsci.2013.06.004, 2013.

Fullgraf, T., Zammit, C., Bailly, L., Terrier, M., Hyvonen, E., Backman, B., Karinen, T., Konnunaho, J., Thomas, R. and Tychsen, J.: Geological Mapping and Mineral Assessment Project (GEMMAP) of Malawi. Report Inception Phase - February 2017., 2017.

Gaherty, J. B., Zheng, W., Shillington, D. J., Pritchard, M. E., Henderson, S. T., Chindandali, P. R. N., Mdala, H., Shuler, A., Lindsey, N., Oliva, S. J., Nooner, S., Scholz, C. A., Schaff, D., Ekström, G. and Nettles, M.: Faulting processes during early-stage rifting: Seismic and geodetic analysis of the 2009-2010 Northern Malawi earthquake sequence, Geophys. J. Int., 217(3), 1767–1782, doi:10.1093/gji/ggz119, 2019.

Goda, K., Gibson, E. D., Smith, H. R., Biggs, J. and Hodge, M.: Seismic risk assessment of urban and rural settlements around lake malawi, Front. Built Environ., 2, doi:10.3389/fbuil.2016.00030, 2016.

Goda, K., Kloukinas, P., Risi, R., Hodge, M., Kafodya, I., Ngoma, I., Biggs, J., Crewe, A., Fagereng, Å. and Macdonald, J.: Scenario-based seismic risk assessment for Malawi using improved information on earthquake sources and local building characteristics, in 16th European Conference on Earthquake Engineering, pp. 1–12., 2018.

Goitom, B., Werner, M. J., Goda, K., Kendall, J. M., Hammond, J. O. S., Ogubazghi, G., Oppenheimer, C., Helmstetter, A., Keir, D. and Illsley-Kemp, F.: Probabilistic seismic-hazard assessment for Eritrea, Bull. Seismol. Soc. Am., 107(3), 1478–1494, doi:10.1785/0120160210, 2017.

Gómez-Vasconcelos, M. G., Villamor, P., Procter, J., Palmer, A., Cronin, S., Wallace, C., Townsend, D. and Leonard, G.: Characterisation of faults as earthquake sources from geomorphic data in the Tongariro Volcanic Complex, New Zealand, New Zeal. J. Geol. Geophys., 1–12, 2018.

Gupta, H. K.: The Malawi earthquake of March 10, 1989: A report of the macroseismic survey, Tectonophysics, 209(1–4), 165–166, doi:10.1016/0040-1951(92)90018-2, 1992.

Gupta, S., Cowie, P. A., Dawers, N. H. and Underhill, J. R.: A mechanism to explain rift-basin subsidence and stratigraphic patterns through fault-array evolution, Geology, 26(7), 595–598, doi:10.1130/0091-7613(1998)026<0595:AMTERB>2.3.CO, 1998.

Habgood, F., Holt, D. N. and Walshaw, R. D.: The geology of the Thyolo Area, Bull. Geol. Surv. Malawi, 22, 1973.

Hamiel, Y., Baer, G., Kalindekafe, L., Dombola, K. and Chindandali, P.: Seismic and aseismic slip evolution and deformation associated with the 2009-2010 northern Malawi earthquake swarm, East African Rift, Geophys. J. Int., 191(3), 898–908, doi:10.1111/j.1365-246X.2012.05673.x, 2012.

Harris, R. A.: Introduction to Special Section: Stress Triggers, Stress Shadows, and Implications for Seismic Hazard, J. Geophys. Res. Solid Earth, 103(B10), 24347–24358, doi:10.1029/98jb01576, 1998.

Hart, E. and Bryant, W.: Fault-rupture hazard zones in California: Alquist-Priolo Earthquake Fault Zoning Act with Index to Earthquake Fault Zones Maps., 1997.

Heimpel, M. and Olson, P.: A seismodynamical model of lithosphere deformation: Development of continental and oceanic rift networks, J. Geophys. Res. Solid Earth, 101(B7), 16155–16176, doi:10.1029/96jb00168, 1996.

Hellebrekers, N., Niemeijer, A. R., Fagereng, Å., Manda, B. and Mvula, R. L. S.: Lower crustal

https://doi.org/10.5194/se-2020-104
Preprint. Discussion started: 14 July 2020



earthquakes in the East African Rift System: Insights from frictional properties of rock samples from the Malawi rift, Tectonophysics, 767, 228167, doi:10.1016/j.tecto.2019.228167, 2019.

Hemphill-Haley, M. A. and Weldon, R. J.: Estimating prehistoric earthquake magnitude from point measurements of surface rupture, Bull. Seismol. Soc. Am., 89(5), 1264–1279, 1999.

Hodge, M., Biggs, J., Goda, K. and Aspinall, W.: Assessing infrequent large earthquakes using geomorphology and geodesy: the Malawi Rift, Nat. Hazards, 76(3), 1781–1806, doi:10.1007/s11069-014-1572-y, 2015.

Hodge, M., Fagereng, A., Biggs, J. and Mdala, H.: Controls on Early-Rift Geometry: New Perspectives From the Bilila-Mtakataka Fault, Malawi, Geophys. Res. Lett., 45(9), 3896–3905, doi:10.1029/2018GL077343, 2018a.

Hodge, M., Fagereng and Biggs, J.: The Role of Coseismic Coulomb Stress Changes in Shaping the Hard Link Between Normal Fault Segments, J. Geophys. Res. Solid Earth, 123(1), 797–814, doi:10.1002/2017JB014927, 2018b.

Hodge, M., Biggs, J., Fagereng, A., Elliott, A., Mdala, H. and Mphepo, F.: A semi-automated algorithm to quantify scarp morphology (SPARTA): Application to normal faults in southern Malawi, Solid Earth, 10(1), 27–57, doi:10.5194/se-10-27-2019, 2019.

Hodge, M., Biggs, J., Fagereng, Mdala, H., Wedmore, L. N. J. and Williams, J. N.: Evidence From High-Resolution Topography for Multiple Earthquakes on High Slip-to-Length Fault Scarps: The Bilila-Mtakataka Fault, Malawi, Tectonics, 39(2), e2019TC005933, doi:10.1029/2019TC005933, 2020.

Iezzi, F., Roberts, G., Walker, J. F. and Papanikolaou, I.: Occurrence of partial and total coseismic ruptures of segmented normal fault systems: Insights from the Central Apennines, Italy., J. Struct. Geol., doi:10.1016/j.jsg.2019.05.003, 2019.

Ivory, S. J., Blome, M. W., King, J. W., McGlue, M. M., Cole, J. E. and Cohen, A. S.: Environmental change explains cichlid adaptive radiation at Lake Malawi over the past 1.2 million years, Proc. Natl. Acad. Sci. U. S. A., 113(42), 11895–11900, doi:10.1073/pnas.1611028113, 2016.

Jackson, J.: Living with earthquakes: Know your faults, J. Earthq. Eng., 5, 5–123, doi:10.1080/13632460109350530, 2001.

Jackson, J. and Blenkinsop, T.: The Malaŵi Earthquake of March 10, 1989: Deep faulting within the East African Rift System, Tectonics, 12(5), 1131–1139, doi:10.1029/93TC01064, 1993.

Jackson, J. and Blenkinsop, T.: The Bilila-Mtakataka fault in Malawi: an active, 100-km long, normal fault segment in thick seismogenic crust, Tectonics, 16(1), 137–150, doi:10.1029/96TC02494, 1997.

Jackson, J. A. and White, N. J.: Normal faulting in the upper continental crust: observations from regions of active extension, J. Struct. Geol., 11(1–2), 15–36, doi:10.1016/0191-8141(89)90033-3, 1989.

Jomard, H., Marc Cushing, E., Palumbo, L., Baize, S., David, C. and Chartier, T.: Transposing an active fault database into a seismic hazard fault model for nuclear facilities - Part 1: Building a database of potentially active faults (BDFA) for metropolitan France, Nat. Hazards Earth Syst. Sci., doi:10.5194/nhess-17-1573-2017, 2017.

Keir, D., Ebinger, C. J., Stuart, G. W., Daly, E. and Ayele, A.: Strain accommodation by magmatism and faulting as rifting proceeds to breakup: Seismicity of the northern Ethiopian rift, J. Geophys. Res. Solid Earth, 111(5), doi:10.1029/2005JB003748, 2006.

King, A. W. and Dawson, A. L.: The Geology of the Mangochu-Makanjila Area, Bull. Geol. Surv. Malawi, 35, 1976.

https://doi.org/10.5194/se-2020-104
Preprint. Discussion started: 14 July 2020


Kloukinas, P., Novelli, V., Kafodya, I., Ngoma, I., Macdonald, J. and Goda, K.: A building classification scheme of housing stock in Malawi for earthquake risk assessment, J. Hous. Built Environ., 1–31, doi:10.1007/s10901-019-09697-5, 2019.

Kolawole, F., Atekwana, E. A., Laó-Dávila, D. A., Abdelsalam, M. G., Chindandali, P. R., Salima, J. and Kalindekafe, L.: Active Deformation of Malawi Rift's North Basin Hinge Zone Modulated by Reactivation of Preexisting Precambrian Shear Zone Fabric, Tectonics, 37(3), 683–704, doi:10.1002/2017TC004628, 2018a.

Kolawole, F., Atekwana, E. A., Laó-Dávila, D. A., Abdelsalam, M. G., Chindandali, P. R., Salima, J. and Kalindekafe, L.: High-resolution electrical resistivity and aeromagnetic imaging reveal the causative fault of the 2009 Mw 6.0 Karonga, Malawi earthquake, Geophys. J. Int., 213(2), 1412–1425, doi:10.1093/gji/ggy066, 2018b.

Koyi, H. A., Hessami, K. and Teixell, A.: Epicenter distribution and magnitude of earthquakes in fold-thrust belts: Insights from sandbox models, Geophys. Res. Lett., 27(2), 273–276, doi:10.1029/1999GL010833, 2000.

Kröner, A., Willner, A. P., Hegner, E., Jaeckel, P. and Nemchin, A.: Single zircon ages, PT evolution and Nd isotopic systematics of high-grade gneisses in southern Malawi and their bearing on the evolution of the Mozambique belt in southeastern Africa, Precambrian Res., 109(3–4), 257–291, doi:10.1016/S0301-9268(01)00150-4, 2001.

Langridge, R. M., Ries, W. F., Litchfield, N. J., Villamor, P., Van Dissen, R. J., Barrell, D. J. A., Rattenbury, M. S., Heron, D. W., Haubrock, S., Townsend, D. B., Lee, J. M., Berryman, K. R., Nicol, A., Cox, S. C. and Stirling, M. W.: The New Zealand Active Faults Database, New Zeal. J. Geol. Geophys., 59(1), 86–96, doi:10.1080/00288306.2015.1112818, 2016.

Laõ-Dávila, D. A., Al-Salmi, H. S., Abdelsalam, M. G. and Atekwana, E. A.: Hierarchical

https://doi.org/10.5194/se-2020-104
Preprint. Discussion started: 14 July 2020




segmentation of the Malawi Rift: The influence of inherited lithospheric heterogeneity and kinematics in the evolution of continental rifts, Tectonics, 34(12), 2399–2417, doi:10.1002/2015TC003953, 2015.

Lavayssière, A., Drooff, C., Ebinger, C., Gallacher, R., Illsley-Kemp, F., Oliva, S. J. and Keir, D.: Depth Extent and Kinematics of Faulting in the Southern Tanganyika Rift, Africa, Tectonics, 38(0), doi:10.1029/2018TC005379, 2019.

Leonard, M.: Earthquake fault scaling: Self-consistent relating of rupture length, width, average displacement, and moment release, Bull. Seismol. Soc. Am., 100(5 A), 1971–1988, doi:10.1785/0120090189, 2010.

Litchfield, N., Wyss, B., Christophersen, A., Thomas, R., Berryman, K., Henshaw, P. and Villamor, P.: Guidelines for compilation of neotectonic faults, folds and fault sources, GEM Faulted Earth [online] Available from: www.nexus.globalquakemodel.org/gem-faulted-earth/posts/, 2013.

Litchfield, N., Van Dissen, R., Sutherland, R., Barnes, P., Cox, S., Norris, R., Beavan, R., Langridge, R., Villamor, P., Berryman, K., Stirling, M., Nicol, A., Nodder, S., Lamarche, G., Barrell, D., Pettinga, J., Little, T., Pondard, N., Mountjoy, J. and Clark, K.: A model of active faulting in New Zealand, New Zeal. J. Geol. Geophys., 57(1), 32–56, doi:10.1080/00288306.2013.854256, 2014.

Litchfield, N. J., Villamor, P., van Dissen, R. J., Nicol, A., Barnes, P. M., Barrell, D. J. A., Pettinga, J. R., Langridge, R. M., Little, T. A., Mountjoy, J. J., Ries, W. F., Rowland, J., Fenton, C., Stirling, M. W., Kearse, J., Berryman, K. R., Cochran, U. A., Clark, K. J., Hemphill-Haley, M., Khajavi, N., Jones, K. E., Archibald, G., Upton, P., Asher, C., Benson, A., Cox, S. C., Gasston, C., Hale, D., Hall, B., Hatem, A. E., Heron, D. W., Howarth, J., Kane, T. J., Lamarche, G., Lawson, S., Lukovic, B., McColl, S. T., Madugo, C., Manousakis, J., Noble, D., Pedley, K., Sauer, K., Stahl, T., Strong,

D. T., Townsend, D. B., Toy, V., Williams, J., Woelz, S. and Zinke, R.: Surface rupture of multiple crustal faults in the 2016 Mw 7.8 Kaikōura, New Zealand, earthquake, Bull. Seismol. Soc. Am., 108(3B), 1496–1520, doi:10.1785/0120170300, 2018.

Lyons, R. P., Scholz, C. A., Cohen, A. S., King, J. W., Brown, E. T., Ivory, S. J., Johnson, T. C., Deino, A. L., Reinthal, P. N., McGlue, M. M. and Blome, M. W.: Continuous 1.3-million-year record of East African hydroclimate, and implications for patterns of evolution and biodiversity, Proc. Natl. Acad. Sci., 201512864, doi:10.1073/pnas.1512864112, 2015.

Macgregor, D.: History of the development of the East African Rift System: A series of interpreted maps through time, J. African Earth Sci., 101, 232–252, doi:10.1016/j.jafrearsci.2014.09.016, 2015.

Machette, M., Haller, K. and Wald, L.: Quaternary Fault and Fold Database for the nation. United States Geological Survey Fact Sheet. [online] Available from: https://pubs.usgs.gov/fs/2004/3033/FS2004-3033.pdf, 2004.

Macheyeki, A. S., Mdala, H., Chapola, L. S., Manhiça, V. J., Chisambi, J., Feitio, P., Ayele, A., Barongo, J., Ferdinand, R. W., Ogubazghi, G., Goitom, B., Hlatywayo, J. D., Kianji, G. K., Marobhe, I., Mulowezi, A., Mutamina, D., Mwano, J. M., Shumba, B. and Tumwikirize, I.: Active fault mapping in Karonga-Malawi after the December 19, 2009 Ms 6.2 seismic event, J. African Earth Sci., 102, 233–246, doi:10.1016/j.jafrearsci.2014.10.010, 2015.

Malawi National Statistics Office: 2018 Malawi Population & Housing Census Main Report, Gov. Malawi, 2018.

Manda, B. W. C., Cawood, P. A., Spencer, C. J., Prave, T., Robinson, R. and Roberts, N. M. W.: Evolution of the Mozambique Belt in Malawi constrained by granitoid U-Pb, Sm-Nd and Lu-Hf isotopic data, Gondwana Res., 68, 93–107, doi:10.1016/j.gr.2018.11.004, 2019.

Marzocchi, W. and Melini, D.: On the earthquake predictability of fault interaction models, Geophys. Res. Lett., doi:10.1002/2014GL061718, 2014.

Marzocchi, W., Selva, J., Cinti, F. R., Montone, P., Pierdominici, S., Schivardi, R. and Boschi, E.: On the occurrence of large earthquakes: New insights from a model based on interacting faults embedded in a realistic tectonic setting, J. Geophys. Res. Solid Earth, 114(1), doi:10.1029/2008JB005822, 2009.

McCalpin, J. P.: Paleoseismology, Academic press., 2009.

McCartney, T. and Scholz, C. A.: A 1.3 million year record of synchronous faulting in the hangingwall and border fault of a half-graben in the Malawi (Nyasa) Rift, J. Struct. Geol., 91, 114–129, doi:10.1016/j.jsg.2016.08.012, 2016.

Menegon, L., Pennacchioni, G., Malaspina, N., Harris, K. and Wood, E.: Earthquakes as Precursors of Ductile Shear Zones in the Dry and Strong Lower Crust, Geochemistry, Geophys. Geosystems, doi:10.1002/2017GC007189, 2017.

Mesko, G.: Magmatism at the Southern End of the East African Rift System: Origin and Role During Early Stage Rifting, 2020.

Midzi, V., Hlatywayo, D. J., Chapola, L. S., Kebede, F., Atakan, K., Lombe, D. K., Turyomurugyendo, G. and Tugume, F. A.: Seismic hazard assessment in Eastern and Southern Africa, Ann. di Geofis., V42(No 6), 1067–1083, doi:10.4401/ag-3770, 1999.

Molinaro, M., Leturmy, P., Guezou, J. C., Frizon de Lamotte, D. and Eshraghi, S. A.: The structure and kinematics of the southeastern Zagros fold-thrust belt, Iran: From thin-skinned to thick-skinned tectonics, Tectonics, 24(3), 1–19, doi:10.1029/2004TC001633, 2005.

Morley, C. K.: Variable extension in Lake Tanganyika, Tectonics, 7(4), 785–801, doi:10.1029/TC007i004p00785, 1988.

https://doi.org/10.5194/se-2020-104
Preprint. Discussion started: 14 July 2020



Mortimer, E. J., Paton, D. A., Scholz, C. A., Strecker, M. R. and Blisniuk, P.: Orthogonal to oblique rifting: Effect of rift basin orientation in the evolution of the North basin, Malawi Rift, East Africa, Basin Res., 19(3), 393–407, doi:10.1111/j.1365-2117.2007.00332.x, 2007.

Mortimer, E. J., Kirstein, L. A., Stuart, F. M. and Strecker, M. R.: Spatio-temporal trends in normal-fault segmentation recorded by low-temperature thermochronology: Livingstone fault scarp, Malawi Rift, East African Rift System, Earth Planet. Sci. Lett., 455, 62–72, doi:10.1016/j.epsl.2016.08.040, 2016.

Mouthereau, F., Fillon, C. and Ma, K. F.: Distribution of strain rates in the Taiwan orogenic wedge, Earth Planet. Sci. Lett., 284(3–4), 361–385, doi:10.1016/j.epsl.2009.05.005, 2009.

Muirhead, J. D., Kattenhorn, S. A., Lee, H., Mana, S., Turrin, B. D., Fischer, T. P., Kianji, G., Dindi, E. and Stamps, D. S.: Evolution of upper crustal faulting assisted by magmatic volatile release during early-stage continental rift development in the East African Rift, Geosphere, 12(6), 1670–1700, doi:10.1130/GES01375.1, 2016.

Muirhead, J. D., Wright, L. J. M. and Scholz, C. A.: Rift evolution in regions of low magma input in East Africa, Earth Planet. Sci. Lett., 506, 332–346, doi:10.1016/j.epsl.2018.11.004, 2019.

Mynatt, W. G., Beresh, S. C. M., Elifritz, E. A., Johnson, S., Mendez, K., Mayle, M., Atekwana, E. A., Laó-Dávila, D. A., Chindandali, P. R. N. and Chisenga, C.: Imaging of the Subsurface Expression of the Bilila-Mtakataka Fault Using Electrical Resistivity in the Central Malawi Rift, in AGU Fall Meeting Abstracts., 2017.

Ngoma, I., Kafodya, I., Kloukinas, P., Novelli, V., Macdonald, J. and Goda, K.: Building classification and seismic vulnerability of current housing construction in Malawi, Malawi J. Sci. Technol., 11(1), 57–72, 2019.

Nicol, A., Walsh, J. J., Watterson, J. and Underhill, J. R.: Displacement rates of normal faults, Nature, 390(6656), 157–159, doi:10.1038/36548, 1997.

Nicol, A., Walsh, J., Berryman, K. and Villamor, P.: Interdependence of fault displacement rates and paleoearthquakes in an active rift, Geology, 34(10), 865–868, doi:10.1130/G22335.1, 2006.

Nicol, A., Van Dissen, R. J., Stirling, M. W. and Gerstenberger, M. C.: Completeness of the Paleoseismic Active-Fault Record in New Zealand, Seismol. Res. Lett., 87(6), 1299–1310, doi:10.1785/0220160088, 2016a.

Nicol, A., Robinson, R., Van Dissen, R. J. and Harvison, A.: Variability of recurrence interval and single-event slip for surface-rupturing earthquakes in New Zealand, New Zeal. J. Geol. Geophys., 59(1), 97–116, doi:10.1080/00288306.2015.1127822, 2016b.

Novelli, V., Kloukinas, P., De Risi, R., Kafodya, I., Ngoma, I., Macdonald, J. and Goda, K.: Seismic Mitigation Framework for Non-engineered Masonry Buildings in Developing Countries: Application to Malawi in the East African Rift, in Resilient Structures and Infrastructure, pp. 195–223, Springer., 2019.

Nyblade, A. A. and Langston, C. A.: East African earthquakes below 20 km depth and their implications for crustal structure, Geophys. J. Int., 121(1), 49–62, doi:10.1111/j.1365-246X.1995.tb03510.x, 1995.

Olive, J. A., Behn, M. D. and Malatesta, L. C.: Modes of extensional faulting controlled by surface processes, Geophys. Res. Lett., 41(19), 6725–6733, doi:10.1002/2014GL061507, 2014.

Pace, B., Visini, F. and Peruzza, L.: FiSH : MATLAB Tools to Turn Fault Data into Seismic-Hazard Models, Seismol. Res. Lett., 87(2A), 374–386, doi:10.1785/0220150189, 2016.

Parsons, T., Field, E. H., Page, M. T. and Milner, K.: Possible earthquake rupture connections on mapped California faults ranked by calculated Coulomb linking stresses, Bull. Seismol. Soc. Am.,

https://doi.org/10.5194/se-2020-104
Preprint. Discussion started: 14 July 2020



102(6), 2667–2676, doi:10.1785/0120110349, 2012.

De Pascale, G. P., Araya, J., Perisco, M., Sandoval, F., Sepulveda, S. and Moncada, D.: New school faults and seismic hazard, guilty (i.e. active) until proven innocent (i.e. inactive), in PATA DAYS 2017; 8th International Workshop on Paleoseismology, Active Tectonics and Archeoseismology, 13th-16th November 2017, Blenheim, New Zealand., 2017.

Pérouse, E. and Wernicke, B. P.: Spatiotemporal evolution of fault slip rates in deforming continents: The case of the Great Basin region, northern Basin and Range province, Geosphere, 13(1), 112–135, doi:10.1130/GES01295.1, 2017.

Petit, C. and Ebinger, C.: Flexure and mechanical behavior of cratonic lithosphere: Gravity models of the East African and Baikal rifts, J. Geophys. Res. Solid Earth, doi:10.1029/2000JB900101, 2000.

Philippon, M., Willingshofer, E., Sokoutis, D., Corti, G., Sani, F., Bonini, M. and Cloetingh, S.: Slip re-orientation in oblique rifts, Geology, 43(2), 147–150, doi:10.1130/G36208.1, 2015.

Pike, J. G.: A pre-colonial history of Malawi, Nyasal. J., 18(1), 22–54, 1965.

Poblet, J. and Lisle, R. J.: Kinematic evolution and structural styles of fold-and-thrust belts, Geol. Soc. Spec. Publ., 349, 1–24, doi:10.1144/SP349.1, 2011.

Poggi, V., Durrheim, R., Tuluka, G. M., Weatherill, G., Gee, R., Pagani, M., Nyblade, A. and Delvaux, D.: Assessing seismic hazard of the East African Rift: a pilot study from GEM and AfricaArray, Bull. Earthq. Eng., 1–31, doi:10.1007/s10518-017-0152-4, 2017.

Quigley, M., Van Dissen, R., Litchfield, N., Villamor, P., Duffy, B., Barrell, D., Furlong, K., Stahl, T., Bilderback, E. and Noble, D.: Surface rupture during the 2010 Mw 7.1 darfield(canterbury) earthquake: Implications for fault rupture dynamics and seismic-hazard analysis, Geology, 40(1), 55–58, doi:10.1130/G32528.1, 2012.

https://doi.org/10.5194/se-2020-104
Preprint. Discussion started: 14 July 2020


Rabinowitz, N. and Steinberg, D. M.: Seismic hazard sensitivity analysis: a multi-parameter approach, Bull. - Seismol. Soc. Am., 81(3), 796–817, 1991.

Roberts, E. M., Stevens, N. J., O'Connor, P. M., Dirks, P. H. G. M., Gottfried, M. D., Clyde, W. C., Armstrong, R. A., Kemp, A. I. S. and Hemming, S.: Initiation of the western branch of the East African Rift coeval with the eastern branch, Nat. Geosci., 5(4), 289–294, doi:10.1038/ngeo1432, 2012.

Robertson, E. A. M., Biggs, J., Cashman, K. V., Floyd, M. A. and Vye-Brown, C.: Influence of regional tectonics and pre-existing structures on the formation of elliptical calderas in the Kenyan Rift, in Geological Society Special Publication, vol. 420, pp. 43–67., 2016.

Robinson, R., van Dissen, R. and Litchfield, N.: Using synthetic seismicity to evaluate seismic hazard in the Wellington region, New Zealand, Geophys. J. Int., 187(1), 510–528, doi:10.1111/j.1365-246X.2011.05161.x, 2011.

Rodgers, D. W. and Little, T. A.: World's largest coseismic strike-slip offset: The 1855 rupture of the Wairarapa Fault, New Zealand, and implications for displacement/length scaling of continental earthquakes, J. Geophys. Res. Solid Earth, 111(12), doi:10.1029/2005JB004065, 2006.

Sandwell, D., Mellors, R., Tong, X., Wei, M. and Wessel, P.: Open radar interferometry software for mapping surface Deformation, Eos, Trans. Am. Geophys. Union, doi:10.1029/2011EO280002, 2011.

Saria, E., Calais, E., Altamimi, Z., Willis, P. and Farah, H.: A new velocity field for Africa from combined GPS and DORIS space geodetic Solutions: Contribution to the definition of the African reference frame (AFREF), J. Geophys. Res. Solid Earth, 118(4), 1677–1697, doi:10.1002/jgrb.50137, 2013.

Saria, E., Calais, E., Stamps, D. S., Delvaux, D. and Hartnady, C. J. H.: Present-day kinematics of

https://doi.org/10.5194/se-2020-104
Preprint. Discussion started: 14 July 2020

Solid Earth Discussions

the East African Rift, J. Geophys. Res. Solid Earth, 119(4), 3584–3600, doi:10.1002/2013JB010901, 2014.

Scholz, C. A.: Seismic Atlas of Lake Malawi (Nyasa), East Africa, Project PROBE, Duke University., 1989.

Scholz, C. H.: The Mechanics of Earthquakes and Faulting, 2nd ed., Cambridge University Press, Cambridge., 2002.

Scholz, C. H. and Contreras, J. C.: Mechanics of continental rift architecture, Geology, 26(11), 967–970, doi:10.1130/0091-7613(1998)026<0967:MOCRA>2.3.CO, 1998.

Shillington, D. J., Gaherty, J. B., Ebinger, C. J., Scholz, C. A., Selway, K., Nyblade, A. A., Bedrosian, P. A., Class, C., Nooner, S. L. and Pritchard, M. E.: Acquisition of a unique onshore/offshore geophysical and geochemical dataset in the Northern Malawi (Nyasa) Rift, Seismol. Res. Lett., 87(6), 1406–1416, 2016.

Shillington, D. J., Scholz, C. A., Chindandali, P. R. N., Gaherty, J. B., Accardo, N. J., Onyango, E., Ebinger, C. J. and Nyblade, A. A.: Controls on rift faulting in the North Basin of the Malawi (Nyasa) Rift, East Africa, Tectonics, e2019TC005633, doi:10.1029/2019tc005633, 2020.

Shudofsky, G. N., Cloetingh, S., Stein, S. and Wortel, R.: Unusually deep earthquakes in East Africa: Constraints on the thermo-mechanical structure of a continental rift system, Geophys. Res. Lett., 14(7), 741–744, doi:10.1029/GL014i007p00741, 1987.

Shyu, J. B. H., Chuang, Y. R., Chen, Y. L., Lee, Y. R. and Cheng, C. T.: A new on-land seismogenic structure source database from the Taiwan earthquake model (TEM) project for seismic hazard analysis of Taiwan, Terr. Atmos. Ocean. Sci., 27(3), 311–323, doi:10.3319/TAO.2015.11.27.02(TEM), 2016.

https://doi.org/10.5194/se-2020-104
Preprint. Discussion started: 14 July 2020



Sibson, R. H.: Earthquake faulting as a structural process, J. Struct. Geol., 11(1–2), 1–14, doi:10.1016/0191-8141(89)90032-1, 1989.

Smekalin, O., Chipizubov, A. and Imaev, V.: Paleoearthquakes in the Baikal region: Methods and results of timing, Geotectonics, 44(2), 158–175, doi:10.1134/s0016852110020056, 2010.

Stahl, K.: Some notes on the development of Zomba, Soc. Malawi J., 63(2), 39–55, 2010.

Stamps, D. S., Calais, E., Saria, E., Hartnady, C., Nocquet, J. M., Ebinger, C. J. and Fernandes, R. M.: A kinematic model for the East African Rift, Geophys. Res. Lett., 35(5), doi:10.1029/2007GL032781, 2008.

Stamps, D. S., Saria, E. and Kreemer, C.: A Geodetic Strain Rate Model for the East African Rift System, Sci. Rep., 8(1), doi:10.1038/s41598-017-19097-w, 2018.

Stein, S., Geller, R. J. and Liu, M.: Why earthquake hazard maps often fail and what to do about it, Tectonophysics, doi:10.1016/j.tecto.2012.06.047, 2012.

Stirling, M., McVerry, G., Gerstenberger, M., Litchfield, N., Van Dissen, R., Berryman, K., Barnes, P., Wallace, L., Villamor, P., Langridge, R., Lamarche, G., Nodder, S., Reyners, M., Bradley, B., Rhoades, D., Smith, W., Nicol, A., Pettinga, J., Clark, K. and Jacobs, K.: National seismic hazard model for New Zealand: 2010 update, Bull. Seismol. Soc. Am., 102(4), 1514–1542, doi:10.1785/0120110170, 2012.

Stirling, M., Goded, T., Berryman, K. and Litchfield, N.: Selection of earthquake scaling relationships for seismic-hazard analysis, Bull. Seismol. Soc. Am., 103(6), 2993–3011, doi:10.1785/0120130052, 2013.

Styron, R., García-Pelaez, J. and Pagani, M.: CCAF-DB: The Caribbean and Central American active fault database, Nat. Hazards Earth Syst. Sci., 20(3), 831–857, doi:10.5194/nhess-20-831-

https://doi.org/10.5194/se-2020-104
Preprint. Discussion started: 14 July 2020




2020, 2020.

Taylor-Silva, B. I., Stirling, M. W., Litchfield, N. J., Griffin, J. D., van den Berg, E. J. and Wang, N.: Paleoseismology of the Akatore Fault, Otago, New Zealand, New Zeal. J. Geol. Geophys., 1–17, doi:10.1080/00288306.2019.1645706, 2019.

Taylor, M. and Yin, A.: Active structures of the Himalayan-Tibetan orogen and their relationships to earthquake distribution, contemporary strain field, and Cenozoic volcanism, Geosphere, 5(3), 199–214, doi:10.1130/GES00217.1, 2009.

Turcotte, D. L. and Schubert, G.: Geodynamics: Applications of continuum physics to geological problems, 450 pp, 1982.

U.S. Department of the Interior U.S. Geological Survey: M 5.5 - 24km NE of Nsanje, Malawi [available at https://earthquake.usgs.gov/earthquakes/eventpage/us1000d1cy#executive, last accessed 26 Sept 2018], 2018.

Valentini, A., DuRoss, C. B., Field, E. H., Gold, R. D., Briggs, R. W., Visini, F. and Pace, B.: Relaxing Segmentation on the Wasatch Fault Zone: Impact on Seismic Hazard, Bull. Seismol. Soc. Am., 110(1), 83–109, doi:10.1785/0120190088, 2020.

Vallage, A. and Bollinger, L.: Testing Fault Models in Intraplate Settings: A Potential for Challenging the Seismic Hazard Assessment Inputs and Hypothesis?, Pure Appl. Geophys., 1–11, doi:10.1007/s00024-019-02129-z, 2019.

Villamor, P., Litchfield, N., Barrell, D., Van Dissen, R., Hornblow, S., Quigley, M., Levick, S., Ries, W., Duffy, B., Begg, J., Townsend, D., Stahl, T., Bilderback, E., Noble, D., Furlong, K. and Grant, H.: Map of the 2010 Greendale Fault surface rupture, Canterbury, New Zealand: Application to land use planning, New Zeal. J. Geol. Geophys., 55(3), 223–230, doi:10.1080/00288306.2012.680473, 2012.

https://doi.org/10.5194/se-2020-104
Preprint. Discussion started: 14 July 2020

Solid Earth Discussions

Villamor, P., Barrell, D. J. A., Gorman, A., Davy, B., Hreinsdóttir, S., Hamling, I. J., Stirling, M. W., Cox, S. C., Litchfield, N. J., Holt, A., Todd, E., Denys, P., Pearson, C., C, S., Garcia-Mayordomo, J., Goded, T., Abbot, E., Ohneiser, C., Lepine, P. and F, C.-T.: Unknown faults under cities, Lower Hutt., 2018.

Vittori, E., Delvaux, D. and Kervyn, F.: Kanda fault: A major seismogenic element west of the Rukwa Rift (Tanzania, East Africa), J. Geodyn., 24(1–4), 139–153, doi:10.1016/S0264-3707(96)00038-5, 1997.

Wallace, L. M., Barnes, P., Beavan, J., Van Dissen, R., Litchfield, N., Mountjoy, J., Langridge, R., Lamarche, G. and Pondard, N.: The kinematics of a transition from subduction to strike-slip: An example from the central New Zealand plate boundary, J. Geophys. Res. Solid Earth, 117(2), doi:10.1029/2011JB008640, 2012.

Wallace, R. W.: Degradation of the Hebgen Lake fault scarps of 1959., Geology, 8(5), 225–229, doi:10.1130/0091-7613(1980)8<225:DOTHLF>2.0.CO;2, 1980.

Walsh, J. J., Nicol, A. and Childs, C.: An alternative model for the growth of faults, J. Struct. Geol., 24(11), 1669–1675, doi:10.1016/S0191-8141(01)00165-1, 2002.

Walshaw, R. D.: The Geology of the Nchue-Balaka Area, Bull. Geol. Surv. Malawi, 19, 1965.

Walter, J.: The Geology of the Salima-Mvera Mission Area, Bull. Geol. Surv. Malawi, 30, 1972.

Wang, T., Feng, J., Liu, K. H. and Gao, S. S.: Crustal structure beneath the Malawi and Luangwa Rift Zones and adjacent areas from ambient noise tomography, Gondwana Res., 67, 187–198, doi:10.1016/j.gr.2018.10.018, 2019.

Wedmore, L. N. J., Faure Walker, J. P., Roberts, G. P., Sammonds, P. R., McCaffrey, K. J. W. and Cowie, P. A.: A 667 year record of coseismic and interseismic Coulomb stress changes in central

https://doi.org/10.5194/se-2020-104
Preprint. Discussion started: 14 July 2020



Italy reveals the role of fault interaction in controlling irregular earthquake recurrence intervals, J. Geophys. Res. Solid Earth, 122(7), 5691–5711, doi:10.1002/2017JB014054, 2017.

Wedmore, L. N. J., Biggs, J., Williams, J. N., Fagereng, Å., Dulanya, Z., Mphepo, F. and Mdala, H.: Active fault scarps in southern Malawi and their implications for the distribution of strain in incipient continental rifts, Tectonics, e2019TC005834, doi:10.1029/2019TC005834, 2020a.

Wedmore, L. N. J., Williams, J. N., Biggs, J., Fagereng, A., Mphepo, F., Dulanya, Z., Willoughby, J., Mdala, H. and Adams, B.: Depth-dependent controls on structure, reactivation and geomorphology of the active Thyolo border fault, Malawi rift, , doi:https://doi.org/10.31223/osf.io/4bs9x, 2020b.

Wells, D. L. and Coppersmith, K. J.: New Empirical Relationships among Magnitude, Rupture Length, Rupture Width, Rupture Area, and Surface Displacement, Bull. Seismol. Soc. Am., 84(4), 974–1002, doi:<p></p>, 1994.

Wesnousky, S. G.: Displacement and geometrical characteristics of earthquake surface ruptures: Issues and implications for seismic-hazard analysis and the process of earthquake rupture, Bull. Seismol. Soc. Am., 98(4), 1609–1632, doi:10.1785/0120070111, 2008.

Wessel, B., Huber, M., Wohlfart, C., Marschalk, U., Kosmann, D. and Roth, A.: Accuracy assessment of the global TanDEM-X Digital Elevation Model with GPS data, ISPRS J. Photogramm. Remote Sens., 139, 171–182, 2018.

Wheeler, W. H. and Rosendahl, B. R.: Geometry of the Livingstone Mountains Border Fault, Nyasa (Malawi) Rift, East Africa, Tectonics, 13(2), 303–312, doi:10.1029/93TC02314, 1994.

Willemse, E. J. M.: Segmented normal faults: Correspondence between three-dimensional mechanical models and field data, J. Geophys. Res. Solid Earth, 102(B1), 675–692, 1997.

https://doi.org/10.5194/se-2020-104
Preprint. Discussion started: 14 July 2020


Williams, J. N., Fagereng, Å., Wedmore, L. N. J., Biggs, J., Mphepo, F., Dulanya, Z., Mdala, H. and Blenkinsop, T.: How Do Variably Striking Faults Reactivate During Rifting? Insights From Southern Malawi, Geochemistry, Geophys. Geosystems, 20(7), 3588–3607, doi:10.1029/2019GC008219, 2019.

World Bank: Tectonic Shift : Rift 2018 - Regional Seismic Risk and Resilience Workshop (English). [online] Available from: http://documents.worldbank.org/curated/en/325121555063464245/Tectonic-Shift-Rift-2018-Regional-Seismic-Risk-and-Resilience-Workshop, 2019.

WorldPop: www.worldpop.org - School of Geography and Environmental Science, University of Southampton; Department of Geography and Geosciences, University of Louisville; Departement de Geographie, Universite de Namur) and Center for International Earth Science Info, , doi:DOI: 10.5258/SOTON/WP00538, 2018.

Wright, L. J. M., Muirhead, J. D. and Scholz, C. A.: Spatio-temporal variations in upper crustal extension across the different basement terranes of the Lake Tanganyika Rift, East Africa, Tectonics, doi:10.1029/2019tc006019, 2020.

Zeng, Y. and Shen, Z. K.: Fault network modeling of crustal deformation in California constrained using GPS and geologic observations, Tectonophysics, 612–613, 1–17, doi:10.1016/j.tecto.2013.11.030, 2014.

Zhang, P., Slemmons, D. B. and Mao, F.: Geometric pattern, rupture termination and fault segmentation of the Dixie Valley-Pleasant Valley active normal fault system, Nevada, U.S.A., J. Struct. Geol., 13(2), 165–176, doi:10.1016/0191-8141(91)90064-P, 1991.

Zielke, O. and Strecker, M. R.: Recurrence of large earthquakes in magmatic continental rifts: Insights from a paleoseismic study along the Laikipia-Marmanet fault, Subukia Valley, Kenya rift, Bull. Seismol. Soc. Am., 99(1), 61–70, doi:10.1785/0120080015, 2009.

https://doi.org/10.5194/se-2020-104
Preprint. Discussion started: 14 July 2020




## List of Figures

### Figure 1

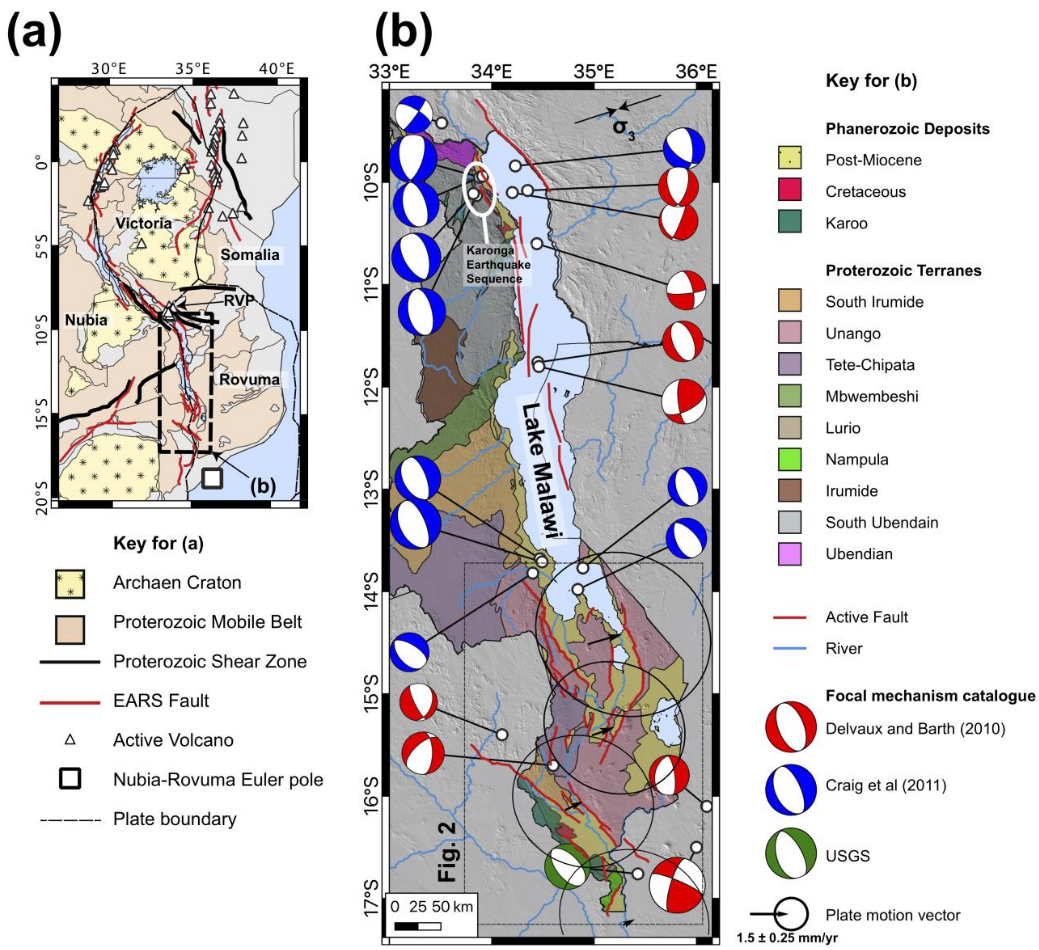


Figure 1: (a) Location of the Malawi within East Africa. Distribution of Archean Cratons, Proterozoic Mobile Belts and shear zones modified after Fritz et al., (2013), major faults in the East African Rift modified after Hodge et al., (2018). and Macgregor, (2015). Plate boundaries and the Euler pole between the Nubia and Rovuma plates after Saria et al., (2013). RVP; Rungwe Volcanic Province. (b) Simplified geological map of Malawi, with Proterozoic Terranes after Fullgraf et al., (2017). Map is underlain by Shuttle Radar Topography Mission (STRM) 30-m digital elevation

https://doi.org/10.5194/se-2020-104
Preprint. Discussion started: 14 July 2020


model (DEM; Sandwell et al., 2011). Extent of Fig. 2 also shown. Active faults within this area are those included in the South Malawi Active Fault Database (SMAFD). Active faults outside this region mapped as in (a). Focal mechanisms collated from Delvaux and Barth, (2010), Craig et al., (2011), and U.S. Department of the Interior U.S. Geological Survey, (2018). Minimum principal compressive stress ($\sigma_3$) trend from focal mechanism stress inversion (Williams et al., 2019). Plate motion vector for central point of each graben in southern Malawi (Fig. A2) for Nubia-Rovuma Euler pole (Saria et al., 2013), modelled using methods described in Robertson et al., (2016).

https://doi.org/10.5194/se-2020-104
Preprint. Discussion started: 14 July 2020


Solid Earth Discussions
Open Access
EGU

1633 **Figure 2**

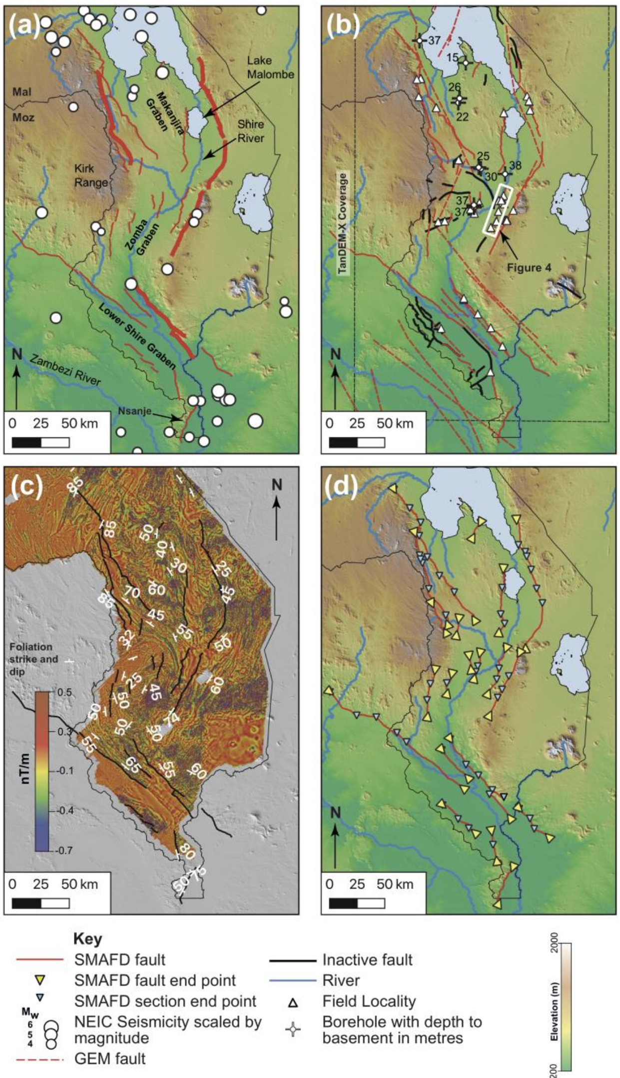


1634

1635 Figure 2: (a) Active fault map for south Malawi underlain by SRTM 30 m resolution DEM, division

1636 of its principal grabens (with border faults heavily weighted), and National Earthquake Information

1637 Centre (NEIC) record for events Mw>2.5 from 1900-February 2019 also shown. (b) Information on

1638 methods used to collate the South Malawi Active Fault Database (SMAFD) and previous fault

1639 mapping (c) Aeromagnetic image created from the vertical derivative. Combined with foliation

https://doi.org/10.5194/se-2020-104
Preprint. Discussion started: 14 July 2020



orientations digitised from geological maps (Bloomfield, 1958, 1965; Bloomfield and Garson, 1965b; Habgood et al., 1973; Walshaw, 1965), and underlain with the SMAFD faults shown in black. For full details of the acquisition of the aeromagnetic data, see Laõ-Dávila et al., (2015). (d) The SMAFD faults and section geometry. Extent of all maps is equivalent and is outlined in Fig. 1b. GEM: Global Earthquake Model, Mal: Malawi, Moz: Mozambique.

https://doi.org/10.5194/se-2020-104
Preprint. Discussion started: 14 July 2020




**Figure 3**

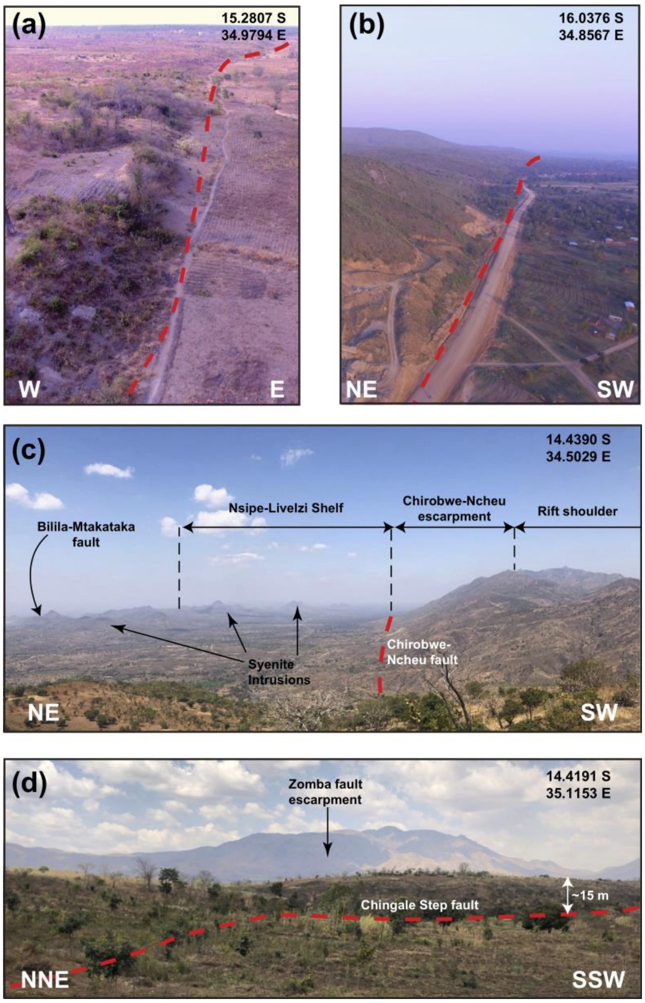


Figure 3: Field examples of border and intrabasinal faults in southern Malawi. Unmanned Aerial Vehicle (UAV) images of scarps (dashed red line) along (a) intrabasinal Mlungusi fault in the Zomba Graben, and (b) the Thyolo fault, the border fault for the Lower Shire Graben. (c) View across the western edge of the Makanjira Graben showing the Chirobwe Ncheu and Bilila-Mtakataka faults, and Proterozoic syenite intrusions (Walshaw, 1965). (d) Minor step in the scarp along the intrabasinal Chingale Step fault, with the escarpment of the Zomba border fault behind.

https://doi.org/10.5194/se-2020-104
Preprint. Discussion started: 14 July 2020




1654 **Figure 4**

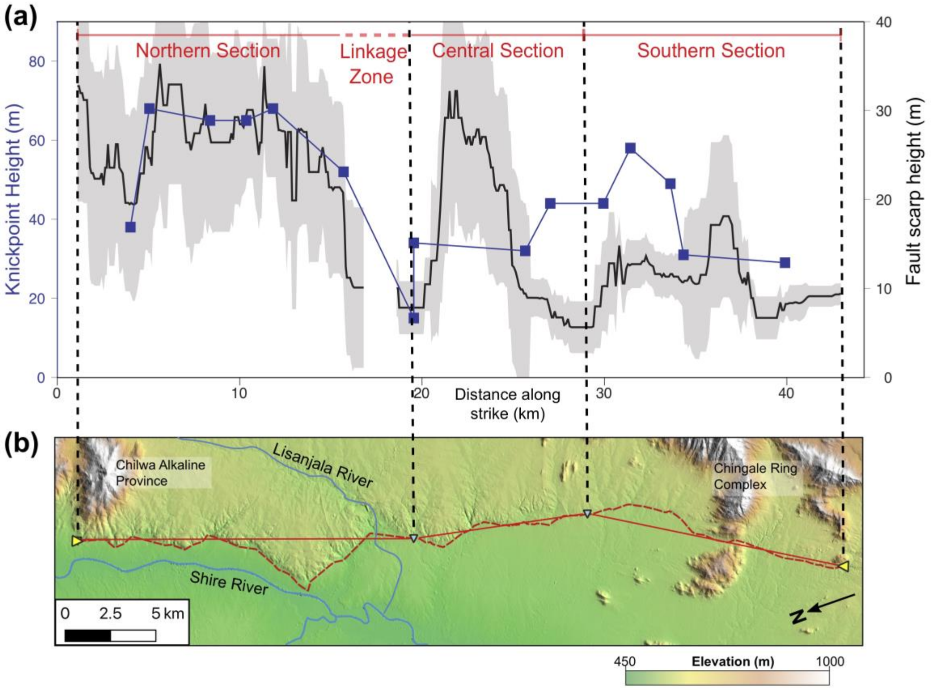


1655

1656 Figure 4: Fault segmentation along the Chingale Step fault, modified after Wedmore et al., (2020a).
1657 (a) Along strike variation in stream knickpoint (blue points) and fault scarp height (black line), with
1658 the gap due to erosion by the Lisanjala River. Grey shading represents one standard deviation error
1659 in scarp height measurements (Wedmore et al., 2020a). (b) Map of Chingale Step fault underlain by
1660 TanDEM-X DEM, extent of area shown in Fig. 2b. The dashed red line shows the surface trace of
1661 the fault. The solid red line shows the geometry of the fault used in earthquake source modelling,
1662 where it is defined by straight lines between section endpoints (blue triangles). An along-strike scarp
1663 height minima at the boundary between the northern and central section occurs at a bend in the fault
1664 scarp, however, there is no obvious geometrical complexity at the along strike scarp height minima
1665 between the southern and central sections. Topography associated with the Proterozoic Chingale
1666 Ring Structure and Chilwa Alkaline Province (Bloomfield, 1965; Manda et al., 2019) is also
1667 indicated. For full details on (a) see Wedmore et al., (2020a).

https://doi.org/10.5194/se-2020-104
Preprint. Discussion started: 14 July 2020


**Figure 5**

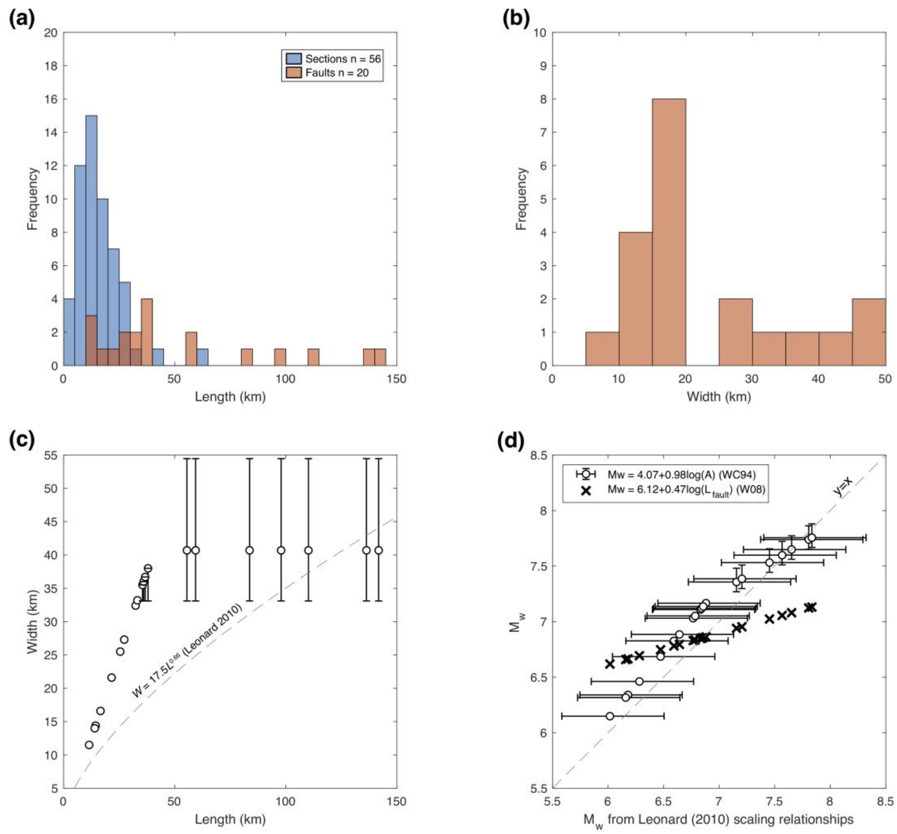


Figure 5: Assessment of fault geometry in the SMAFD. Histograms showing distribution of (a) fault ($L_{fault}$) and section ($L_{sec}$) lengths, and (b) fault widths (*W*) in the SMAFD. The latter is derived from the Leonard, (2010) scaling relationship (Eq. (2)), and in (c) the predicted aspect ratio of faults following this relationship (dashed grey line) is compared to an alternative method to estimate *W* using Eq. (1) (white circles). (d) A comparison of empirical scaling relationships used to estimate earthquake magnitudes ($M_W$) from fault geometry in the SMAFD. Leonard, (2010) magnitudes estimated using Eq. (4), with error bars representing range of $C_1$ and $C_2$ values derived for interplate dip-slip faults. *A*, fault area calculated from $L_{fault}$ and *W* using Eq. (1); WC 94, Wells and Coppersmith (1994); W08, Wesnousky (2008).

https://doi.org/10.5194/se-2020-104
Preprint. Discussion started: 14 July 2020



**Figure 6**

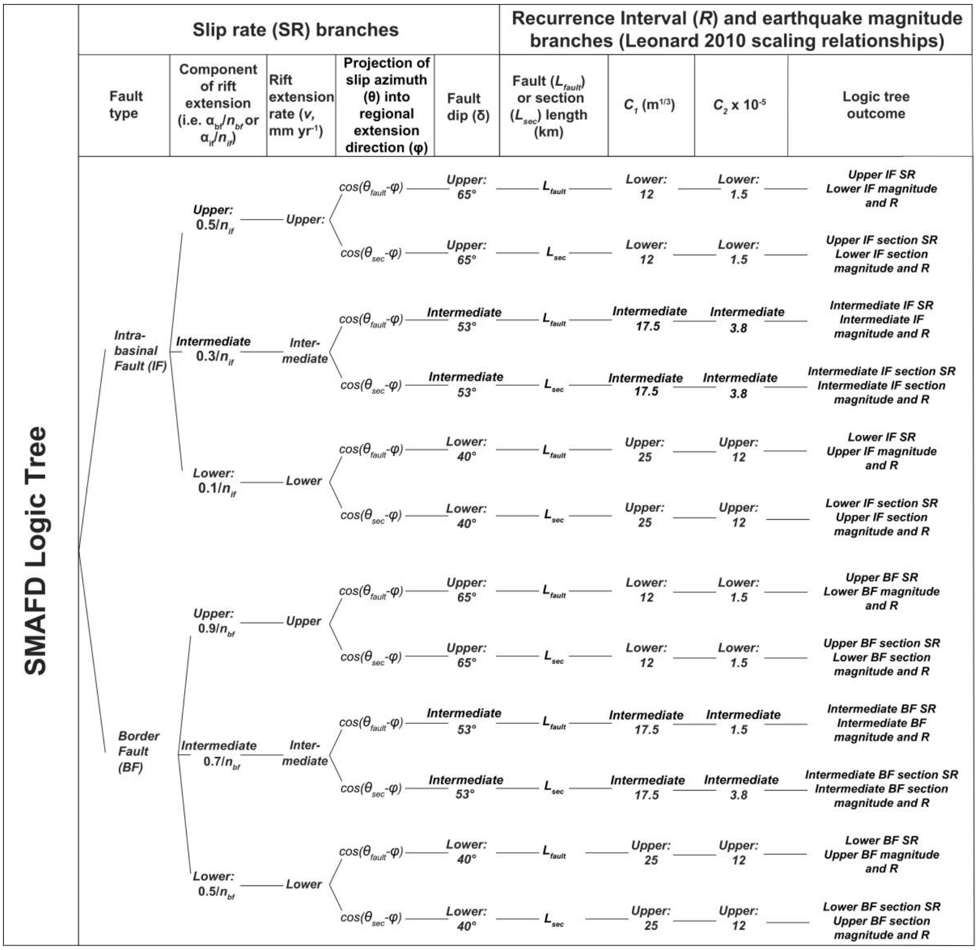


Figure 6: Logic tree for calculating lower, intermediate, and upper estimates of fault slip rates and earthquake magnitudes and recurrence intervals in the SMAFD; $\alpha_{bf}$ and $\alpha_{if}$ are the rift extension weighting assigned to border faults and intrabasinal faults respectively; $n_{bf}$ and $n_{if}$ are the number of border or intrabasinal faults in a graben, $\theta_{fault}$ and $\theta_{sec}$ are whole fault and individual section slip azimuth.

https://doi.org/10.5194/se-2020-104
Preprint. Discussion started: 14 July 2020

Solid Earth Discussions
Open Access

**Figure 7**

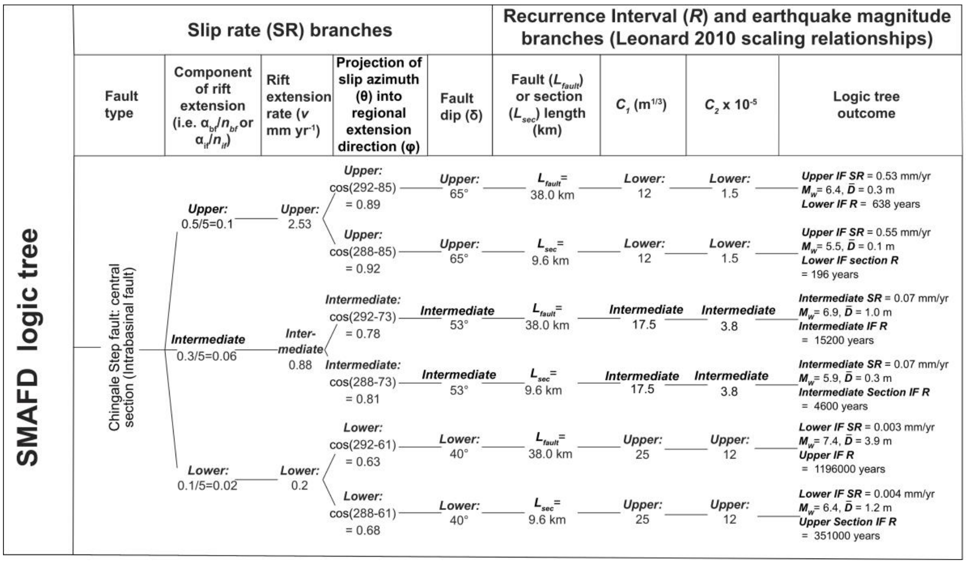


Figure 7: Example of the calculations in the SMAFD logic tree (Fig. 6), performed for the central section of the Chingale Step Fault (Fig. 4b). This is an intrabasinal fault in the Zomba Graben, where the number of intrabasinal faults ($n_{if}$) is five. A multiparameter sensitivity analysis for these calculations is documented in Appendix B.

**Figure 8**

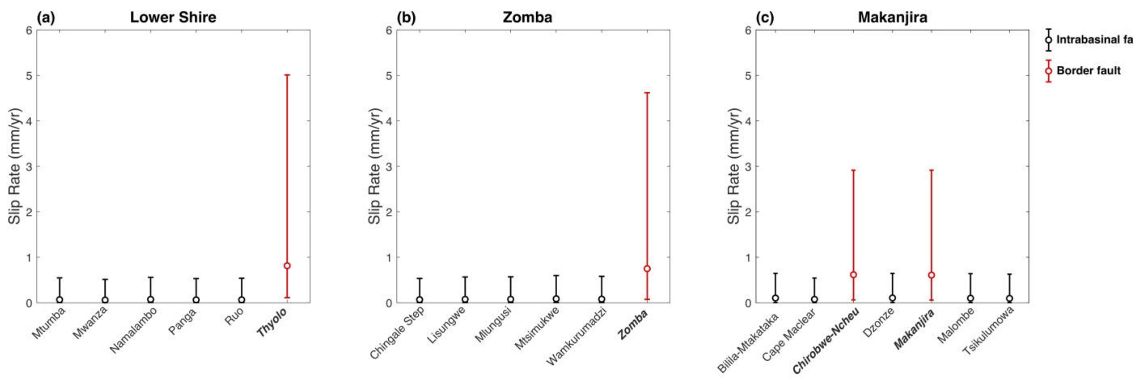


Figure 8: Fault slip rate estimates in the SMAFD, calculated following approach outlined in Fig. 6 for faults in (a) Lower Shire graben, (b) Zomba graben, and (c) Makanjira graben. Middle point represents intermediate estimate with error bars representing upper and lower estimates. Faults with red data points, and names that are bold and italicised are classified as border faults in the SMAFD, the remaining faults are intrabasinal.

https://doi.org/10.5194/se-2020-104
Preprint. Discussion started: 14 July 2020




**Figure 9**

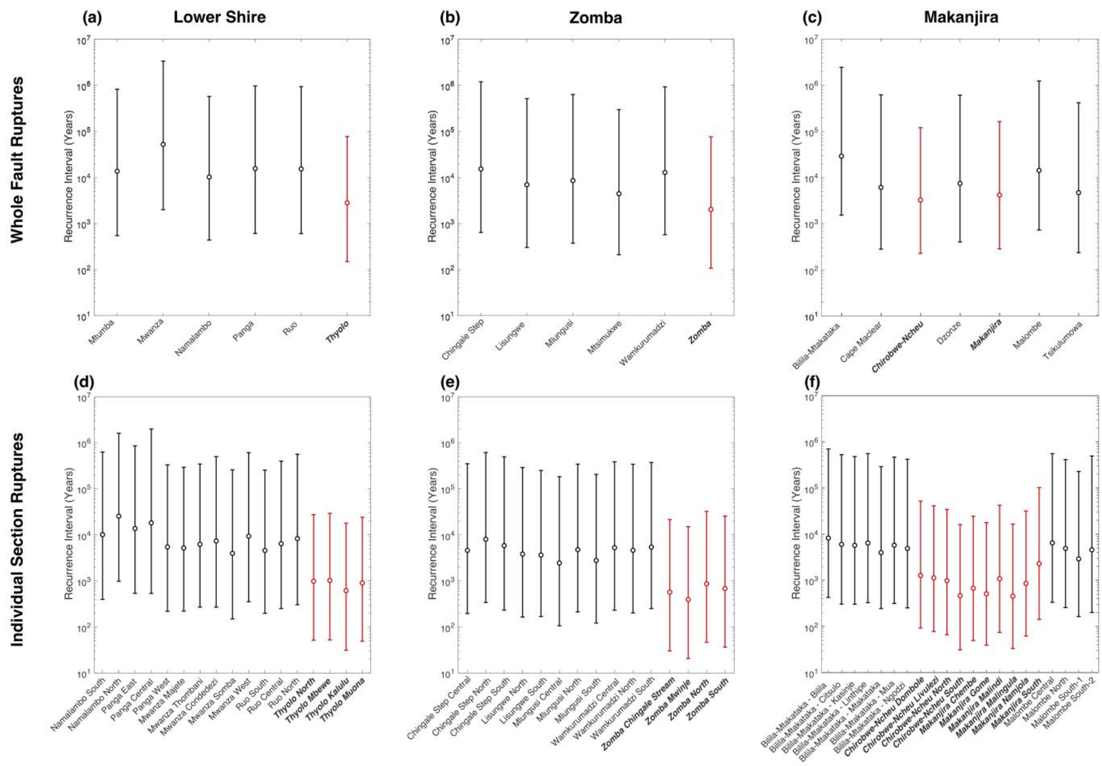


1702

1703 Figure 9: Recurrence interval estimates in the SMAFD for (a-c) whole fault ruptures and (d-f)
1704 individual fault section ruptures. Calculated following approach outlined in Fig. 6, with middle point
1705 representing intermediate estimate, and error bars representing lower and upper estimates. Faults that
1706 are bold and italicised are classified as border faults.

https://doi.org/10.5194/se-2020-104
Preprint. Discussion started: 14 July 2020


**Figure 10**

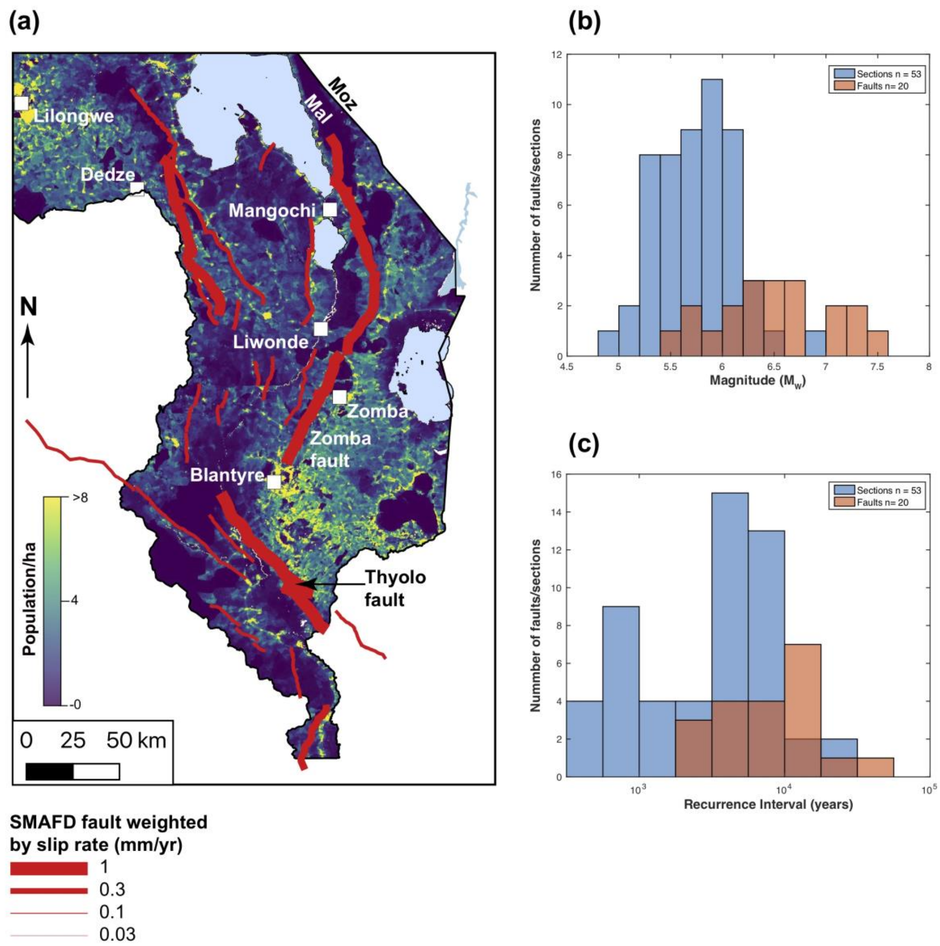


Figure 10: (a) Faults in the SMAFD with lines weighted by intermediate estimates of fault slip rate. Fault map is underlain by population density where the pixel size is 3 arcseconds (approximately 1 ha) as derived from WorldPop predicted 2020 datasets for Malawi (WorldPop, 2018) with major population centres also highlighted. Note that population density in these places may exceed 100 people/ha. Area shown is same as in Fig. 2. Histograms to show range of (b) earthquake magnitudes and (c) recurrence interval estimates in the SMAFD from intermediate branches in Fig. 6.

https://doi.org/10.5194/se-2020-104
Preprint. Discussion started: 14 July 2020


**Figure A1**

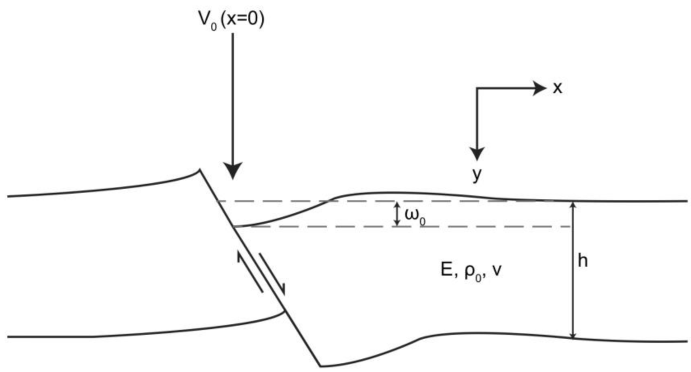


Figure A1: Set-up for hanging wall deflection equations. A vertical load ($V_0$) is applied to the point where the hanging-wall intersects the surface (i.e. where $x$=0) and where there is a maximum deflection ($\omega_0$). The elastic thickness, Young's Modulus, density, and Poisson's ratio of the crust are represented by $h$, $E$, $\rho_0$, and $v$ respectively.

https://doi.org/10.5194/se-2020-104
Preprint. Discussion started: 14 July 2020

Solid Earth Discussions

1723 **Figure A2**

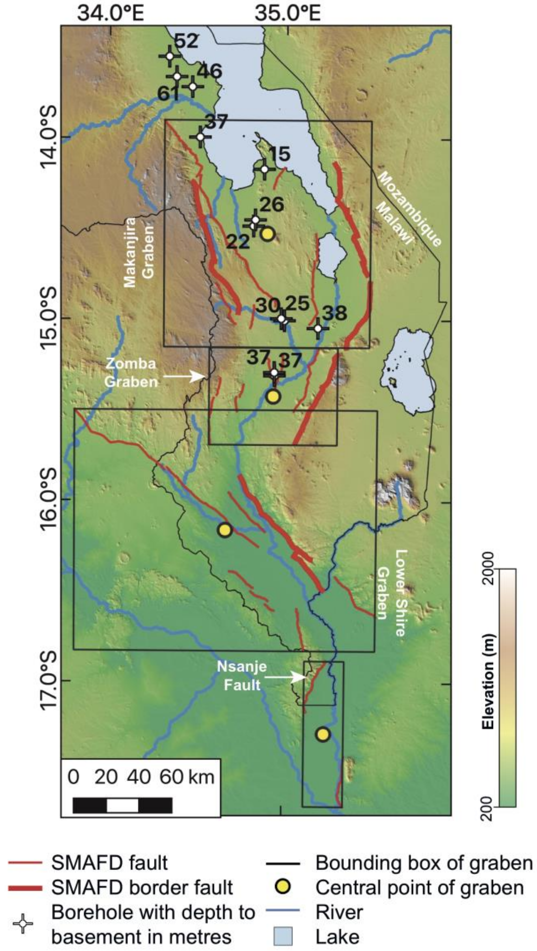


1724

1725 Figure A2: Active fault map for southern Malawi showing respective extent of grabens, their border
1726 faults, and the central point of each graben from which the Nubia-Rovuma plate motion vectors were
1727 derived. Location of boreholes that penetrate basement also shown (Bloomfield and Garson, 1965b;
1728 Walshaw, 1965; Walter, 1972). Map underlain by 30 m resolution Shuttle Radar Topographic
1729 Mission digital elevation model.

https://doi.org/10.5194/se-2020-104
Preprint. Discussion started: 14 July 2020


**Figure A3**

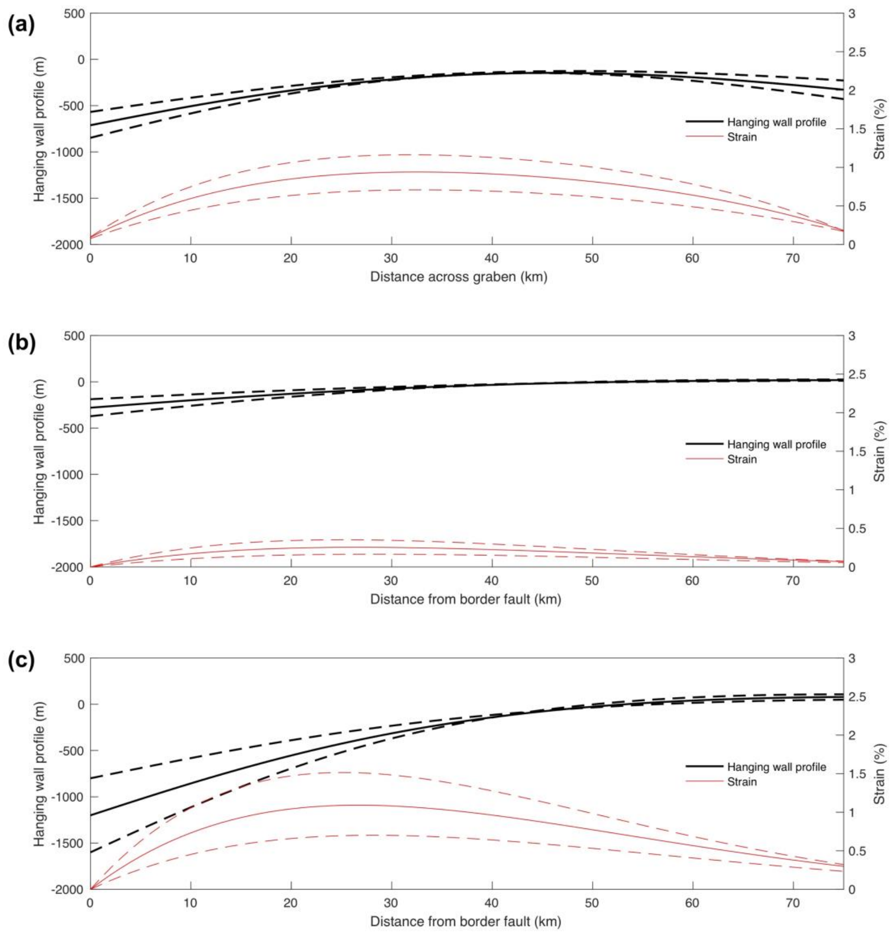


Figure A3: Flexural profiles and horizontal extensional strain for (a) Makanjira, (b) Zomba, and (c) Lower Shire grabens, calculated following methods described in Appendix A and parameters listed in Table A1. Solid line indicates median estimates, dashed line indicates maximum and minimum estimates. For (a), profile shows flexure from both sides of the Makanjira graben and is shown left to right in a WSW-ESE section. Flexural profile is relative to point of zero hanging-wall deflection, not absolute elevation.

https://doi.org/10.5194/se-2020-104
Preprint. Discussion started: 14 July 2020


**Figure B1**

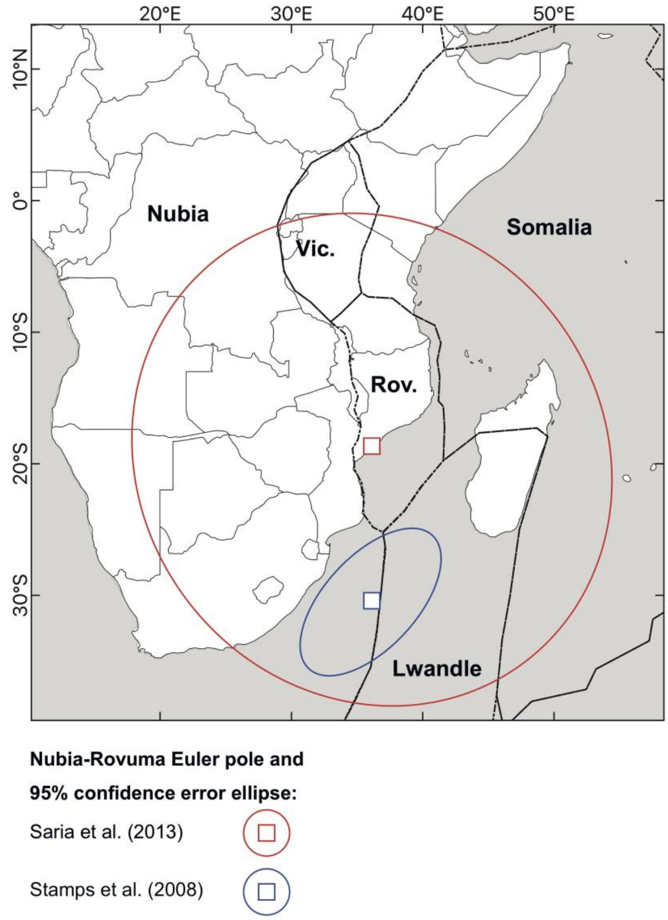


Figure B1: Plate boundaries in East Africa with location and uncertainty of the Nubia-Rovuma Euler pole derived by Saria et al. (2013) and Stamps et al. (2008). Vic., Victoria; Rov., Rovuma. Modified after Saria et al. (2013).

https://doi.org/10.5194/se-2020-104
Preprint. Discussion started: 14 July 2020


**Figure B2**

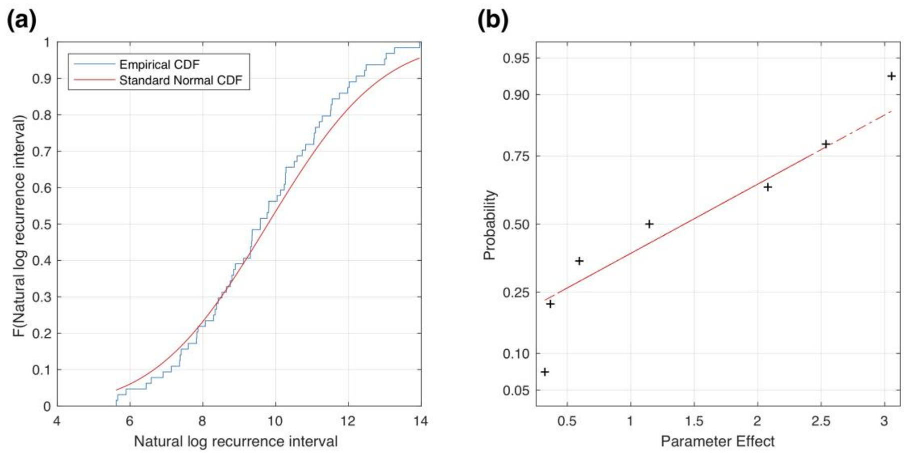


Figure B1: (a) Cumulative distribution function (CDF) of the natural log of the recurrence intervals calculated for the Chingale Step fault central section using the various parameter combinations listed in Table B1 (blue line). This CDF is compared to a standard normal CDF (red line) with the same mean value and standard deviation as the values in Table B1. (b) Normal probability plot of the parameter effects assessed in the sensitivity analysis and reported in Table 4. The most important effects are those that plot above a standard normal distribution (red line). Line is solid when within first and third quartiles of data and dashed when outside.

https://doi.org/10.5194/se-2020-104
Preprint. Discussion started: 14 July 2020



## List of Tables

**Table 1**

| **Attribute type and hierarchical assignment** | **Attribute** | **Type** | **Description** | **Notes** |
|---|---|---|---|---|
| Trace: assigned by trace | Trace ID | Numeric, assigned | Unique two-digit numerical reference ID for each trace | |
| | Fault Name | Text | Fault that trace belongs to. | Assigned based on previous mapping or local geographic feature. |
| | Graben | Text | Graben that fault is located within. | Used in slip rate calculations. |
| | Geomorphic Expression | Text | Geomorphological feature used to identify and map fault trace. | E.g. scarp, escarpment |
| | Location Method | Text | Dataset used to map trace. | E.g. type of digital elevation model |
| | Scale | Numeric, assigned | Coarsest scale at which trace can be mapped. | Reflects the prominence of the fault's geomorphic expression. |
| | Confidence | Numeric, assigned | Score between 1-4 that geomorphic feature used to map trace is an active fault. | |
| | Trace notes | Text | Any remaining miscellaneous geomorphological information about fault trace. | |
| | Author | Text | Fault trace mapper | |
| Section and fault geometry: assigned by section or fault | Section Name | Text | | Assigned based on previous mapping, local geographic feature, or location along fault. |
| | Section Length ($L_{sec}$) | Numeric, assigned | Straight-line distance between section tips. | Measured in km. Except for linking sections, must be >5 km. |
| | Fault Length ($L_{fault}$) | Numeric, assigned | Straight-line distance between fault tips or sum of $L_{sec}$ for segmented faults. | Measured in km |

https://doi.org/10.5194/se-2020-104
Preprint. Discussion started: 14 July 2020

Solid Earth
Discussions

| | | | | |
|---|---|---|---|---|
| | Section strike | Numeric, assigned | Measured from section tips, using bearing that is <180°. | |
| | Fault strike | Numeric, assigned | Measured from fault tips using bearing <180°. | For segmented (i.e. non-planar) this is an 'averaged' value of fault geometry, which is required for slip rate estimates (Eq. (3)). |
| | Dip (δ) | Numeric, assigned | | Attribute parameterised by a set of representative values (40, 53, 65°). |
| | Dip Direction | Text | Compass quadrant that fault dips in. | |
| | Fault Width ($W$) | Numeric, calculated | Calculated from Eq. (2) from Leonard, (2010) scaling relationship using $L_{fault}$. | Not equivalent to rupture width for individual section earthquakes. |
| Kinematic and earthquake source information: assigned by section and/or fault | Section net slip rate | Numeric, calculated | Calculated from Eq. (3). | In mm/yr. All faults in the SMAFD assumed to be normal, so is equivalent to dip-slip rate. |
| | Fault net slip rate | Numeric, calculated | Calculated from Eq. (3). | In mm/yr. All faults in the SMAFD assumed to be normal, so is equivalent to dip-slip rate. Different from section net slip rate where fault strike ≠ section strike. |
| | Section earthquake magnitude | Numeric, calculated | Calculated from Leonard, (2010) scaling relationship using Eq. (4) and $L_{sec}$. | |
| | Fault earthquake magnitude | Numeric, calculated | Calculated from Leonard, (2010) scaling relationship using Eq. (4) and $L_{fault}$. | |
| | Section earthquake recurrence interval ($R$) | Numeric, calculated | Calculated from Eq. (6) and using $L_{sec}$ to calculate average single event displacement in Eq. (5). | |
| | Fault earthquake recurrence interval ($R$) | Numeric, calculated | Calculated from Eq. (6) and using $L_{fault}$ to calculate average single | |

| | | | | |
|---|---|---|---|---|
| | | | event displacement in Eq. (5). | |
| Miscellaneous attributes: assigned by fault | Last event | Text | | Currently this is unknown for all faults in southern Malawi but can be updated when new information becomes available. |
| | Data completeness | Numeric, assigned | Assessment of quality of data and level of knowledge. Score between 1-4, where 1 indicates high completeness. | |
| | Fault notes | Text | Remaining miscellaneous information about fault. | Includes whether fault is classified as a border fault. |
| | References | Text | Relevant geological maps/literature where fault has been previously described. | |
| | Date last updated | Date | | |
| | Compiler | Text | | Not necessarily the same as the fault trace mapper. |

Table 1: List and brief description of attributes in the SMAFD. Representative values for numeric attributes are reported in Table 3.

https://doi.org/10.5194/se-2020-104
Preprint. Discussion started: 14 July 2020


**Table 2**

| Graben | Centre of graben longitude (E) | Centre of graben latitude (S) | Geodetic Model | Velocity and velocity uncertainty of plate motion (mm/yr) | Azimuth, and azimuthal uncertainty of plate motion |
|---|---|---|---|---|---|
| Makanjira | 34.89 | 14.52 | S13 | 1.08 ± 1.66 | 075° ± 089° |
| | | | S08 | 3.01 ± 0.28 | 085º ± 002º |
| Zomba | 34.93 | 15.42 | S13 | 0.88 ± 1.65 | 072° ± 110° |
| | | | S08 | 2.84 ± 0.28 | 085º ± 002º |
| Lower Shire | 34.66 | 16.16 | S13 | 0.74 ± 1.63 | 063° ± 131° |
| | | | S08 | 2.71 ± 0.28 | 084º ± 002º |
| Nsanje | 35.23 | 17.28 | S13 | 0.46 ± 1.63 | 063° ± 212° |
| | | | S08 | 2.49 ± 0.27 | 086º ± 002º |

Table 2: Coordinates from which the Nubia-Rovuma plate motion vector for each graben in southern Malawi was derived (Fig. 1b). The velocity, azimuth, and uncertainties of each vector is also reported given the Nubia-Rovuma Euler poles reported in Saria et al. (2013) (S13), or in Stamps et al., (2008) (S08; Fig. B1), and where the uncertainties associated with the Euler pole are derived from the methods presented in Robertson et al. (2016). For justification of graben centre locations, see Fig. A2.

https://doi.org/10.5194/se-2020-104
Preprint. Discussion started: 14 July 2020


**Table 3**

| **Attribute** | **Minimum** | **Median** | **Maximum** |
|---|---|---|---|
| Section Length ($L_{sec}$, km) | 3.0 | 13.9 | 62.4 |
| Fault Length ($L_{fault}$, km) | 11.5 | 35.7 | 141.8 |
| Fault Width ($W$, km) | 8.9 | 19.0 | 47.6 |
| Section net slip rate (mm/yr) | 0.03 | 0.10 | 0.84 |
| Fault net slip rate (mm/yr) | 0.06 | 0.13 | 0.81 |
| Section earthquake magnitude (Mw) | 5.4 | 6.2 | 7.2 |
| Fault earthquake magnitude (Mw) | 6.0 | 6.8 | 7.8 |
| Section earthquake recurrence interval ($R$, years) | 390 | 4580 | 25500 |
| Fault earthquake recurrence interval ($R$, years) | 2000 | 7190 | 52200 |

Table 3: Range of selected numeric attributes across all faults and sections in the SMAFD. To demonstrate how calculated attributes vary across different faults in the SMAFD, as opposed to variation from the set of parameters used to calculate them, the values shown are for the intermediate branches in the SMAFD logic tree (Fig. 6).

https://doi.org/10.5194/se-2020-104
Preprint. Discussion started: 14 July 2020


1774 **Table 4**

| Parameter | Lower Level | Upper Level | Parameter Main Effect (*A*) |
|---|---|---|---|
| **Component of regional extensional strain ($\alpha_{if}/n_{if}$)** | 0.1 | 0.02 | 3.05 |
| **Rift extension rate (*v*, mm/yr)** | 2.53 | 0.2 | 2.54 |
| **Rift extension azimuth (ϕ)** | 085° | 061° | 0.32 |
| **Fault dip (δ)** | 65° | 40° | 0.59 |
| **Leonard, (2010) empirically derived scaling parameter $C_1$ ($m_{1/3}$)** | 12 | 25 | 0.37 |
| **Leonard, (2010) empirically derived scaling parameter $C_2$** | 1.5 | 12 | 2.08 |
| **Rupture length (*L*, km)** | 9.6 (individual section, $L_{sec}$) | 38.0 (whole fault, $L_{fault}$) | 1.15 |

1775 Table 4: Parameters and their associated upper and lower levels used in the sensitivity analysis for
1776 recurrence interval (*R*) calculations for the Chingale Step fault central section. The main effect of
1777 each parameter is then also reported. See Appendix B for full details of this analysis.

1778

https://doi.org/10.5194/se-2020-104
Preprint. Discussion started: 14 July 2020




**Table A1**

| **Half graben** | **Sediment thickness (m)** | **Escarpment height (m)** | **Border fault throw (m)** | **$\omega_0$ (m)** | **Elastic plate thickness (km)** | **Mean extension (%)** | **Total horizontal extension (m)** | **Half-graben age (Ma)** | **Total flexural extension rate (mm/yr)** | **Flexural extension rate per fault (mm/yr)[1]** |
|---|---|---|---|---|---|---|---|---|---|---|
| **North Basin[2]** | | | | | | $3.8^{+2.8}_{-1.3}$ | $1280^{+6}_{-5}$ | | | |
| **Makanjira (East)** | 70±40[3] | 400±100[5] | 470±140 | 370±110 | 32.5±2.5 | 0.7±0.2 | 510±120 | 4.6-25[7] | $0.035^{+0}_{-0}$ | $0.01^{+0.02}_{-0.00}$ |
| **Makanjira (West)** | 70±40[3] | 850±150[5] | 920±190 | 740±150 | 32.5±2.5 | | | | | |
| **Zomba** | 50±15[4] | 300±100[5] | 350±115 | 280±90 | 32.5±2.5 | 0.2±0.1 | 100±40 | 4.6-25[7] | $0.007^{+0}_{-0}$ | $0.001^{+0.}_{-0.}$ |
| **Lower Shire** | | | 1500±500[6] | 1200±400 | 32.5±2.5 | 0.9±0.3 | 430±160 | 4.6-25[7] | $0.015^{+0}_{-0}$ | $0.004^{+0.}_{-0.}$ |

1780 Table A5: Inputs and results of hanging wall flexure analysis. $\omega_0$; maximum hanging-wall deflection
1781 calculated from Eq. A3.[1]Extension rate per fault, calculated from dividing the rift-wide flexural
1782 extension rate by the number of intrabasinal faults along a rift perpendicular transect. [2]Values
1783 reported are median, upper, and lower estimates of hanging-wall flexure along three profiles across

https://doi.org/10.5194/se-2020-104
Preprint. Discussion started: 14 July 2020


the North Basin of Lake Malawi by Shillington et al. (2020). [3]Thickness of sediments in the Bwande-Liwawadze Valley based on electrical resistivity surveys (Mynatt et al., 2017; Walshaw, 1965) and borehole data. (Fig. A2; Bloomfield and Garson, 1965). [4]Thickness of sediments from borehole data within the Shire Plain (Fig. A2; Bloomfield and Garson, 1965). [5]See Laõ-Dávila et al. (2015). For the Zomba Graben, topography associated with Chilwa Alkaline Province intrusion at the northern end of the Zomba Fault is removed. For Makanjira West, incorporates escarpment height from Chirbowe-Ncheu and Bilila-Mtakataka Fault. [6]No boreholes in the Lower Shire Graben penetrated basement (Habgood et al., 1973). See Appendix A for justification of throw estimates used instead. [7]Range of ages from estimates for the onset of East African Rift Western Branch rifting (~25 Ma; Roberts et al., 2012), and the onset of sediment accumulation in Lake Malawi (4.6 Ma; McCartney and Scholz, 2016).

https://doi.org/10.5194/se-2020-104
Preprint. Discussion started: 14 July 2020



1796 **Table B1**

| **Combination** | **Component of regional extension** | ***v* (mm/yr)** | **φ (°)** | **δ** | **C1 ($m^{1/3}$)** | **C2** | ***L* (km)** | **Natural log Recurrence Interval** |
|---|---|---|---|---|---|---|---|---|
| 1 | 0.1 | 2.53 | 85 | 65 | 12 | 12 | 9.6 | 7.37 |
| 2 | 0.02 | 2.53 | 85 | 65 | 12 | 1.5 | 9.6 | 6.90 |
| 3 | 0.1 | 0.2 | 85 | 65 | 12 | 1.5 | 9.6 | 7.83 |
| 4 | 0.02 | 0.2 | 85 | 65 | 12 | 12 | 9.6 | 11.52 |
| 5 | 0.1 | 2.53 | 85 | 65 | 12 | 1.5 | 38 | 6.44 |
| 6 | 0.02 | 2.53 | 85 | 65 | 12 | 12 | 38 | 10.13 |
| 7 | 0.1 | 0.2 | 85 | 65 | 12 | 12 | 38 | 11.06 |
| 8 | 0.02 | 0.2 | 85 | 65 | 12 | 1.5 | 38 | 10.59 |
| 9 | 0.1 | 2.53 | 61 | 65 | 12 | 1.5 | 9.6 | 5.62 |
| 10 | 0.02 | 2.53 | 61 | 65 | 12 | 12 | 9.6 | 9.31 |
| 11 | 0.1 | 0.2 | 61 | 65 | 12 | 12 | 9.6 | 10.24 |
| 12 | 0.02 | 0.2 | 61 | 65 | 12 | 1.5 | 9.6 | 9.77 |
| 13 | 0.1 | 2.53 | 61 | 65 | 12 | 12 | 38 | 8.84 |
| 14 | 0.02 | 2.53 | 61 | 65 | 12 | 1.5 | 38 | 8.37 |
| 15 | 0.1 | 0.2 | 61 | 65 | 12 | 1.5 | 38 | 9.30 |
| 16 | 0.02 | 0.2 | 61 | 65 | 12 | 12 | 38 | 12.99 |
| 17 | 0.1 | 2.53 | 85 | 40 | 12 | 1.5 | 9.6 | 5.89 |
| 18 | 0.02 | 2.53 | 85 | 40 | 12 | 12 | 9.6 | 9.58 |
| 19 | 0.1 | 0.2 | 85 | 40 | 12 | 12 | 9.6 | 10.51 |
| 20 | 0.02 | 0.2 | 85 | 40 | 12 | 1.5 | 9.6 | 10.04 |
| 21 | 0.1 | 2.53 | 85 | 40 | 12 | 12 | 38 | 9.12 |
| 22 | 0.02 | 2.53 | 85 | 40 | 12 | 1.5 | 38 | 8.65 |
| 23 | 0.1 | 0.2 | 85 | 40 | 12 | 1.5 | 38 | 9.57 |
| 24 | 0.02 | 0.2 | 85 | 40 | 12 | 12 | 38 | 13.26 |
| 25 | 0.1 | 2.53 | 61 | 40 | 12 | 12 | 9.6 | 8.29 |
| 26 | 0.02 | 2.53 | 61 | 40 | 12 | 1.5 | 9.6 | 7.82 |
| 27 | 0.1 | 0.2 | 61 | 40 | 12 | 1.5 | 9.6 | 8.75 |
| 28 | 0.02 | 0.2 | 61 | 40 | 12 | 12 | 9.6 | 12.44 |
| 29 | 0.1 | 2.53 | 61 | 40 | 12 | 1.5 | 38 | 7.36 |
| 30 | 0.02 | 2.53 | 61 | 40 | 12 | 12 | 38 | 11.05 |
| 31 | 0.1 | 0.2 | 61 | 40 | 12 | 12 | 38 | 11.98 |
| 32 | 0.02 | 0.2 | 61 | 40 | 12 | 1.5 | 38 | 11.51 |
| 33 | 0.1 | 2.53 | 85 | 65 | 25 | 1.5 | 9.6 | 5.66 |

https://doi.org/10.5194/se-2020-104
Preprint. Discussion started: 14 July 2020



| **Combination** | **Component of regional extension** | ***v* (mm/yr)** | **φ (°)** | **δ** | **C1 ($m_{1/3}$)** | **C2** | ***L* (km)** | **Natural log Recurrence Interval** |
|---|---|---|---|---|---|---|---|---|
| 34 | 0.02 | 2.53 | 85 | 65 | 25 | 12 | 9.6 | 9.35 |
| 35 | 0.1 | 0.2 | 85 | 65 | 25 | 12 | 9.6 | 10.28 |
| 36 | 0.02 | 0.2 | 85 | 65 | 25 | 1.5 | 9.6 | 9.81 |
| 37 | 0.1 | 2.53 | 85 | 65 | 25 | 12 | 38 | 8.89 |
| 38 | 0.02 | 2.53 | 85 | 65 | 25 | 1.5 | 38 | 8.42 |
| 39 | 0.1 | 0.2 | 85 | 65 | 25 | 1.5 | 38 | 9.35 |
| 40 | 0.02 | 0.2 | 85 | 65 | 25 | 12 | 38 | 13.04 |
| 41 | 0.1 | 2.53 | 61 | 65 | 25 | 12 | 9.6 | 8.07 |
| 42 | 0.02 | 2.53 | 61 | 65 | 25 | 1.5 | 9.6 | 7.60 |
| 43 | 0.1 | 0.2 | 61 | 65 | 25 | 1.5 | 9.6 | 8.52 |
| 44 | 0.02 | 0.2 | 61 | 65 | 25 | 12 | 9.6 | 12.21 |
| 45 | 0.1 | 2.53 | 61 | 65 | 25 | 1.5 | 38 | 7.13 |
| 46 | 0.02 | 2.53 | 61 | 65 | 25 | 12 | 38 | 10.82 |
| 47 | 0.1 | 0.2 | 61 | 65 | 25 | 12 | 38 | 11.75 |
| 48 | 0.02 | 0.2 | 61 | 65 | 25 | 1.5 | 38 | 11.28 |
| 49 | 0.1 | 2.53 | 85 | 40 | 25 | 12 | 9.6 | 8.34 |
| 50 | 0.02 | 2.53 | 85 | 40 | 25 | 1.5 | 9.6 | 7.87 |
| 51 | 0.1 | 0.2 | 85 | 40 | 25 | 1.5 | 9.6 | 8.79 |
| 52 | 0.02 | 0.2 | 85 | 40 | 25 | 12 | 9.6 | 12.48 |
| 53 | 0.1 | 2.53 | 85 | 40 | 25 | 1.5 | 38 | 7.40 |
| 54 | 0.02 | 2.53 | 85 | 40 | 25 | 12 | 38 | 11.09 |
| 55 | 0.1 | 0.2 | 85 | 40 | 25 | 12 | 38 | 12.02 |
| 56 | 0.02 | 0.2 | 85 | 40 | 25 | 1.5 | 38 | 11.55 |
| 57 | 0.1 | 2.53 | 61 | 40 | 25 | 1.5 | 9.6 | 6.58 |
| 58 | 0.02 | 2.53 | 61 | 40 | 25 | 12 | 9.6 | 10.27 |
| 59 | 0.1 | 0.2 | 61 | 40 | 25 | 12 | 9.6 | 11.20 |
| 60 | 0.02 | 0.2 | 61 | 40 | 25 | 1.5 | 9.6 | 10.73 |
| 61 | 0.1 | 2.53 | 61 | 40 | 25 | 12 | 38 | 9.81 |
| 62 | 0.02 | 2.53 | 61 | 40 | 25 | 1.5 | 38 | 9.34 |
| 63 | 0.1 | 0.2 | 61 | 40 | 25 | 1.5 | 38 | 10.26 |
| 64 | 0.02 | 0.2 | 61 | 40 | 25 | 12 | 38 | 13.95 |

Table B1: Input parameter combinations and Chingale Step fault central section recurrence intervals using upper and lower values outlined in Table 4, and a fractional factorial approach with $2_{k-p}$

https://doi.org/10.5194/se-2020-104
Preprint. Discussion started: 14 July 2020



combinations where *k* is 7 and *p* is 1. The design of this table (i.e. whether an upper or lower value of each parameter is chosen) is derived from Box et al. (1978) and can be accessed at: https://www.itl.nist.gov/div898/handbook/pri/section3/eqns/2to7m1.txt (date last accessed 30/03/2020).

https://doi.org/10.5194/se-2020-104
Preprint. Discussion started: 14 July 2020




1805 **Table B2**

| **Parameter** | **Lower Level** | **Upper Level** | **S08 Parameter Main Effect (*A*)** | **S13 Parameter Main Effect (*A*)** |
|---|---|---|---|---|
| **Component of regional extensional strain ($\alpha_{if}/n_{if}$)** | 0.1 | 0.02 | 1.88 | 3.05 |
| **Rift extension rate (*v*, mm/yr)** | 2.56 | 3.12 | 0.20 | 2.54 |
| **Rift extension azimuth (ϕ)** | 085° | 061° | 0.32 | 0.32 |
| **Fault dip (δ)** | 65° | 40° | 0.59 | 0.59 |
| **Leonard, (2010) empirically derived scaling parameter $C_1$ ($m_{1/3}$)** | 12 | 25 | 0.37 | 0.37 |
| **Leonard, (2010) empirically derived scaling parameter $C_2$** | 1.5 | 12 | 2.08 | 2.08 |
| **Rupture length (*L*, km)** | 9.6 (individual section, $L_{sec}$) | 38.0 (whole fault, $L_{fault}$) | 1.15 | 1.15 |

https://doi.org/10.5194/se-2020-104
Preprint. Discussion started: 14 July 2020

Solid Earth Discussions
Open Access

Table B2: As for Table 4 with parameters and their associated upper and lower levels used in the sensitivity analysis for the Chingale Step fault central section recurrence interval (*R*) calculations, however, using the Stamps et al. (2008) (S08) Nubia-Rovuma Euler pole instead (Fig. B1). For comparison, the Parameter Main Effect reported in Table 4 for the Saria et al. (2013) (S13) Euler Pole are also shown.

https://doi.org/10.5194/se-2020-104
Preprint. Discussion started: 14 July 2020

Solid Earth Discussions
Open Access
EGU

**Table B3**

| **Parameter** | **Component of regional extension** | ***v* (mm/yr)** | **φ** | **δ** | **C1** | **C2** | **L** |
|---|---|---|---|---|---|---|---|
| **Component of regional extension** | - | | | | | | |
| **v (mm/yr)** | 0.00 | - | | | | | |
| **φ** | 0.00 | 0.00 | - | | | | |
| **δ** | 0.00 | 0.00 | 0.00 | - | | | |
| **C1** | 0.00 | 0.00 | 0.00 | 0.00 | - | | |
| **C2** | 0.00 | 0.00 | 0.00 | 0.00 | 0.00 | - | |
| **L** | 0.00 | 0.00 | 0.00 | 0.00 | 0.00 | 0.00 | - |

Table B3: Results of parameter-parameter interaction effects on sensitivity analysis using approach outlined in Eq. B3. All results are zero (to two decimal places), and so there are no parameter-parameter effects in the sensitivity analysis outlined here.